

Measurement of high- Q^2 neutral current deep inelastic e^+p scattering cross sections with a longitudinally polarised positron beam at HERA

ZEUS Collaboration

Abstract

Measurements of neutral current cross sections for deep inelastic scattering in e^+p collisions at HERA with a longitudinally polarised positron beam are presented. The single-differential cross-sections $d\sigma/dQ^2$, $d\sigma/dx$ and $d\sigma/dy$ and the reduced cross-section $\tilde{\sigma}$ were measured in the kinematic region $Q^2 > 185 \text{ GeV}^2$ and $y < 0.9$, where Q^2 is the four-momentum transfer squared, x the Bjorken scaling variable, and y the inelasticity of the interaction. The measurements were performed separately for positively and negatively polarised positron beams. The measurements are based on an integrated luminosity of 135.5 pb^{-1} collected with the ZEUS detector in 2006 and 2007 at a centre-of-mass energy of 318 GeV. The structure functions \tilde{F}_3 and $F_3^{\gamma Z}$ were determined by combining the e^+p results presented in this paper with previously published e^-p neutral current results. The asymmetry parameter A^+ is used to demonstrate the parity violation predicted in electroweak interactions. The measurements are well described by the predictions of the Standard Model.

The ZEUS Collaboration

H. Abramowicz^{45,ah}, I. Abt³⁵, L. Adamczyk¹³, M. Adamus⁵⁴, R. Aggarwal^{7,c}, S. Antonelli⁴, P. Antonioli³, A. Antonov³³, M. Arneodo⁵⁰, O. Arslan⁵, V. Aushev^{26,27,z}, Y. Aushev^{27,z,aa}, O. Bachynska¹⁵, A. Bamberger¹⁹, A.N. Barakbaev²⁵, G. Barbagli¹⁷, G. Bari³, F. Barreiro³⁰, N. Bartosik¹⁵, D. Bartsch⁵, M. Basile⁴, O. Behnke¹⁵, J. Behr¹⁵, U. Behrens¹⁵, L. Bellagamba³, A. Bertolin³⁹, S. Bhadra⁵⁷, M. Bindi⁴, C. Blohm¹⁵, V. Bokhonov^{26,z}, T. Bold¹³, K. Bondarenko²⁷, E.G. Boos²⁵, K. Borras¹⁵, D. Boscherini³, D. Bot¹⁵, I. Brock⁵, E. Brownson⁵⁶, R. Brugnera⁴⁰, N. Brümmer³⁷, A. Bruni³, G. Bruni³, B. Brzozowska⁵³, P.J. Bussey²⁰, B. Bylsma³⁷, A. Caldwell³⁵, M. Capua⁸, R. Carlin⁴⁰, C.D. Catterall⁵⁷, S. Chekanov¹, J. Chwastowski^{12,e}, J. Ciborowski^{53,al}, R. Ciesielski^{15,h}, L. Cifarelli⁴, F. Cindolo³, A. Contin⁴, A.M. Cooper-Sarkar³⁸, N. Coppola^{15,i}, M. Corradi³, F. Corriveau³¹, M. Costa⁴⁹, G. D'Agostini⁴³, F. Dal Corso³⁹, J. del Peso³⁰, R.K. Dementiev³⁴, S. De Pasquale^{4,a}, M. Derrick¹, R.C.E. Devenish³⁸, D. Dobur^{19,t}, B.A. Dolgo-shein^{33,†}, G. Dolinska²⁷, A.T. Doyle²⁰, V. Drugakov¹⁶, L.S. Durkin³⁷, S. Dusini³⁹, Y. Eisenberg⁵⁵, P.F. Ermolov^{34,†}, A. Eskreys^{12,†}, S. Fang^{15,j}, S. Fazio⁸, J. Ferrando²⁰, M.I. Ferrero⁴⁹, J. Figiel¹², B. Foster^{38,ad}, G. Gach¹³, A. Galas¹², E. Gallo¹⁷, A. Garfagnini⁴⁰, A. Geiser¹⁵, I. Gialas^{21,w}, A. Gizhko^{27,ab}, L.K. Gladilin^{34,ac}, D. Gladkov³³, C. Glasman³⁰, O. Gogota²⁷, Yu.A. Golubkov³⁴, P. Göttlicher^{15,k}, I. Grabowska-Bold¹³, J. Grebenyuk¹⁵, I. Gregor¹⁵, G. Grigorescu³⁶, G. Grzelak⁵³, O. Gueta⁴⁵, M. Guzik¹³, C. Gwenlan^{38,ae}, T. Haas¹⁵, W. Hain¹⁵, R. Hamatsu⁴⁸, J.C. Hart⁴⁴, H. Hartmann⁵, G. Hartner⁵⁷, E. Hilger⁵, D. Hochman⁵⁵, R. Hori⁴⁷, A. Hüttmann¹⁵, Z.A. Ibrahim¹⁰, Y. Iga⁴², R. Ingber⁴⁵, M. Ishitsuka⁴⁶, H.-P. Jakob⁵, F. Januschek¹⁵, T.W. Jones⁵², M. Jünger⁵, I. Kadenko²⁷, B. Kahle¹⁵, S. Kananov⁴⁵, T. Kanno⁴⁶, U. Karshon⁵⁵, F. Karstens^{19,u}, I.I. Katkov^{15,l}, M. Kaur⁷, P. Kaur^{7,c}, A. Keramidis³⁶, L.A. Khein³⁴, J.Y. Kim⁹, D. Kisielewska¹³, S. Kitamura^{48,aj}, R. Klanner²², U. Klein^{15,m}, E. Koffeman³⁶, N. Kondrashova^{27,ab}, O. Kononenko²⁷, P. Kooijman³⁶, Ie. Korol²⁷, I.A. Korzhavina^{34,ac}, A. Kotański^{14,f}, U. Kötz¹⁵, H. Kowalski¹⁵, O. Kuprash¹⁵, M. Kuze⁴⁶, A. Lee³⁷, B.B. Levchenko³⁴, A. Levy⁴⁵, V. Libov¹⁵, S. Limentani⁴⁰, T.Y. Ling³⁷, M. Lisovyi¹⁵, E. Lobodzinska¹⁵, W. Lohmann¹⁶, B. Löhr¹⁵, E. Lohrmann²², K.R. Long²³, A. Longhin^{39,af}, D. Lontkovskiy¹⁵, O.Yu. Lukina³⁴, J. Maeda^{46,ai}, S. Magill¹, I. Makarenko¹⁵, J. Malka¹⁵, R. Mankel¹⁵, A. Margotti³, G. Marini⁴³, J.F. Martin⁵¹, A. Mastroberardino⁸, M.C.K. Mattingly², I.-A. Melzer-Pellmann¹⁵, S. Mergelmeyer⁵, S. Miglioranza^{15,n}, F. Mohamad Idris¹⁰, V. Monaco⁴⁹, A. Montanari¹⁵, J.D. Morris^{6,b}, K. Mujkic^{15,o}, B. Musgrave¹, K. Nagano²⁴, T. Namssoo^{15,p}, R. Nania³, A. Nigro⁴³, Y. Ning¹¹, T. Nobe⁴⁶, D. Notz¹⁵, R.J. Nowak⁵³, A.E. Nuncio-Quiroz⁵, B.Y. Oh⁴¹, N. Okazaki⁴⁷, K. Olkiewicz¹², Yu. Onishchuk²⁷, K. Papageorgiu²¹, A. Parenti¹⁵, E. Paul⁵, J.M. Pawlak⁵³, B. Pawlik¹², P. G. Pelfer¹⁸, A. Pellegrino³⁶, W. Perlański^{53,am}, H. Perrey¹⁵, K. Piotrkowski²⁹, P. Pluciński^{54,an}, N.S. Pokrovskiy²⁵, A. Polini³, A.S. Proskuryakov³⁴, M. Przybycień¹³, A. Raval¹⁵, D.D. Reeder⁵⁶, B. Reisert³⁵, Z. Ren¹¹, J. Repond¹, Y.D. Ri^{48,ak}, A. Robertson³⁸, P. Roloff^{15,n}, I. Rubinsky¹⁵, M. Ruspa⁵⁰, R. Sacchi⁴⁹, U. Samson⁵, G. Sartorelli⁴, A.A. Savin⁵⁶, D.H. Saxon²⁰, M. Schioppa⁸, S. Schlenstedt¹⁶, P. Schleper²², W.B. Schmidke³⁵, U. Schneekloth¹⁵, V. Schönberg⁵, T. Schörner-Sadenius¹⁵, J. Schwartz³¹, F. Sciulli¹¹, L.M. Shcheglova³⁴, R. Shehzadi⁵, S. Shimizu^{47,n}, I. Singh^{7,c}, I.O. Skillicorn²⁰, W. Słomiński^{14,g}, W.H. Smith⁵⁶, V. Sola²², A. Solano⁴⁹, D. Son²⁸, V. Sosnovtsev³³, A. Spiridonov^{15,q}, H. Stadie²², L. Stanco³⁹, N. Stefaniuk²⁷, A. Stern⁴⁵, T.P. Stewart⁵¹, A. Stifutkin³³, P. Stopa¹², S. Suchkov³³, G. Susinno⁸, L. Suszycki¹³, J. Sztuk-

Dambietz²², D. Szuba²², J. Szuba^{15,r}, A.D. Tapper²³, E. Tassi^{8,d}, J. Terrón³⁰, T. Theedt¹⁵, H. Tiecke³⁶, K. Tokushuku^{24,x}, J. Tomaszewska^{15,s}, V. Trusov²⁷, T. Tsurugai³², M. Turcato²², O. Turkot^{27,ab}, T. Tymieniecka^{54,ao}, M. Vázquez^{36,n}, A. Verbytskyi¹⁵, O. Viazlo²⁷, N.N. Vlasov^{19,v}, R. Walczak³⁸, W.A.T. Wan Abdullah¹⁰, J.J. Whitmore^{41,ag}, K. Wichmann¹⁵, L. Wiggers³⁶, M. Wing⁵², M. Wlasenko⁵, G. Wolf¹⁵, H. Wolfe⁵⁶, K. Wrona¹⁵, A.G. Yagües-Molina¹⁵, S. Yamada²⁴, Y. Yamazaki^{24,y}, R. Yoshida¹, C. Youngman¹⁵, O. Zabiegajlov^{27,ab}, A.F. Żarnecki⁵³, L. Zawiejski¹², O. Zenaiev¹⁵, W. Zeuner^{15,n}, B.O. Zhautykov²⁵, N. Zhmak^{26,z}, A. Zichichi⁴, Z. Zolkapli¹⁰, D.S. Zotkin³⁴

- 1 *Argonne National Laboratory, Argonne, Illinois 60439-4815, USA*^A
2 *Andrews University, Berrien Springs, Michigan 49104-0380, USA*
3 *INFN Bologna, Bologna, Italy*^B
4 *University and INFN Bologna, Bologna, Italy*^B
5 *Physikalisches Institut der Universität Bonn, Bonn, Germany*^C
6 *H.H. Wills Physics Laboratory, University of Bristol, Bristol, United Kingdom*^D
7 *Panjab University, Department of Physics, Chandigarh, India*
8 *Calabria University, Physics Department and INFN, Cosenza, Italy*^B
9 *Institute for Universe and Elementary Particles, Chonnam National University,*
10 *Kwangju, South Korea*
11 *Jabatan Fizik, Universiti Malaya, 50603 Kuala Lumpur, Malaysia*^E
12 *Nevis Laboratories, Columbia University, Irvington on Hudson, New York 10027,*
13 *USA*^F
14 *The Henryk Niewodniczanski Institute of Nuclear Physics, Polish Academy of*
15 *Sciences, Krakow, Poland*^G
16 *AGH-University of Science and Technology, Faculty of Physics and Applied Com-*
17 *puter Science, Krakow, Poland*^H
18 *Department of Physics, Jagellonian University, Cracow, Poland*
19 *Deutsches Elektronen-Synchrotron DESY, Hamburg, Germany*
20 *Deutsches Elektronen-Synchrotron DESY, Zeuthen, Germany*
21 *INFN Florence, Florence, Italy*^B
22 *University and INFN Florence, Florence, Italy*^B
23 *Fakultät für Physik der Universität Freiburg i.Br., Freiburg i.Br., Germany*
24 *School of Physics and Astronomy, University of Glasgow, Glasgow, United King-*
25 *dom*^D
26 *Department of Engineering in Management and Finance, Univ. of the Aegean,*
27 *Chios, Greece*
28 *Hamburg University, Institute of Experimental Physics, Hamburg, Germany*^I
29 *Imperial College London, High Energy Nuclear Physics Group, London, United*
30 *Kingdom*^D
31 *Institute of Particle and Nuclear Studies, KEK, Tsukuba, Japan*^J
32 *Institute of Physics and Technology of Ministry of Education and Science of Kaza-*
khstan, Almaty, Kazakhstan
33 *Institute for Nuclear Research, National Academy of Sciences, Kyiv, Ukraine*
34 *Department of Nuclear Physics, National Taras Shevchenko University of Kyiv,*
35 *Kyiv, Ukraine*
36 *Kyungpook National University, Center for High Energy Physics, Daegu, South Ko-*
37 *rea*^K
38 *Institut de Physique Nucléaire, Université Catholique de Louvain, Louvain-la-Neuve,*
39 *Belgium*^L
40 *Departamento de Física Teórica, Universidad Autónoma de Madrid, Madrid,*
41 *Spain*^M
42 *Department of Physics, McGill University, Montréal, Québec, Canada H3A 2T8*^N
43 *Meiji Gakuin University, Faculty of General Education, Yokohama, Japan*^J

- 33 *Moscow Engineering Physics Institute, Moscow, Russia*^O
- 34 *Lomonosov Moscow State University, Skobeltsyn Institute of Nuclear Physics,*
Moscow, Russia^P
- 35 *Max-Planck-Institut für Physik, München, Germany*
- 36 *NIKHEF and University of Amsterdam, Amsterdam, Netherlands*^Q
- 37 *Physics Department, Ohio State University, Columbus, Ohio 43210, USA*^A
- 38 *Department of Physics, University of Oxford, Oxford, United Kingdom*^D
- 39 *INFN Padova, Padova, Italy*^B
- 40 *Dipartimento di Fisica dell' Università and INFN, Padova, Italy*^B
- 41 *Department of Physics, Pennsylvania State University, University Park,*
Pennsylvania 16802, USA^F
- 42 *Polytechnic University, Tokyo, Japan*^J
- 43 *Dipartimento di Fisica, Università 'La Sapienza' and INFN, Rome, Italy*^B
- 44 *Rutherford Appleton Laboratory, Chilton, Didcot, Oxon, United Kingdom*^D
- 45 *Raymond and Beverly Sackler Faculty of Exact Sciences, School of Physics,*
Tel Aviv University, Tel Aviv, Israel^R
- 46 *Department of Physics, Tokyo Institute of Technology, Tokyo, Japan*^J
- 47 *Department of Physics, University of Tokyo, Tokyo, Japan*^J
- 48 *Tokyo Metropolitan University, Department of Physics, Tokyo, Japan*^J
- 49 *Università di Torino and INFN, Torino, Italy*^B
- 50 *Università del Piemonte Orientale, Novara, and INFN, Torino, Italy*^B
- 51 *Department of Physics, University of Toronto, Toronto, Ontario, Canada M5S*
1A7^N
- 52 *Physics and Astronomy Department, University College London, London, United*
Kingdom^D
- 53 *Faculty of Physics, University of Warsaw, Warsaw, Poland*
- 54 *National Centre for Nuclear Research, Warsaw, Poland*
- 55 *Department of Particle Physics and Astrophysics, Weizmann Institute, Rehovot,*
Israel
- 56 *Department of Physics, University of Wisconsin, Madison, Wisconsin 53706, USA*^A
- 57 *Department of Physics, York University, Ontario, Canada M3J 1P3*^N

- A* supported by the US Department of Energy
- B* supported by the Italian National Institute for Nuclear Physics (INFN)
- C* supported by the German Federal Ministry for Education and Research (BMBF),
under contract No. 05 H09PDF
- D* supported by the Science and Technology Facilities Council, UK
- E* supported by an FRGS grant from the Malaysian government
- F* supported by the US National Science Foundation. Any opinion, findings and conclusions or recommendations expressed in this material are those of the authors and do not necessarily reflect the views of the National Science Foundation.
- G* supported by the Polish Ministry of Science and Higher Education as a scientific project No. DPN/N188/DESY/2009
- H* supported by the Polish Ministry of Science and Higher Education and its grants for Scientific Research
- I* supported by the German Federal Ministry for Education and Research (BMBF),
under contract No. 05h09GUF, and the SFB 676 of the Deutsche Forschungsgemeinschaft (DFG)
- J* supported by the Japanese Ministry of Education, Culture, Sports, Science and Technology (MEXT) and its grants for Scientific Research
- K* supported by the Korean Ministry of Education and Korea Science and Engineering Foundation
- L* supported by FNRS and its associated funds (IISN and FRIA) and by an Inter-University Attraction Poles Programme subsidised by the Belgian Federal Science Policy Office
- M* supported by the Spanish Ministry of Education and Science through funds provided by CICYT
- N* supported by the Natural Sciences and Engineering Research Council of Canada (NSERC)
- O* partially supported by the German Federal Ministry for Education and Research (BMBF)
- P* supported by RF Presidential grant N 4142.2010.2 for Leading Scientific Schools, by the Russian Ministry of Education and Science through its grant for Scientific Research on High Energy Physics and under contract No.02.740.11.0244
- Q* supported by the Netherlands Foundation for Research on Matter (FOM)
- R* supported by the Israel Science Foundation

- a* now at University of Salerno, Italy
- b* now at Queen Mary University of London, United Kingdom
- c* also funded by Max Planck Institute for Physics, Munich, Germany
- d* also Senior Alexander von Humboldt Research Fellow at Hamburg University, Institute of Experimental Physics, Hamburg, Germany
- e* also at Cracow University of Technology, Faculty of Physics, Mathematics and Applied Computer Science, Poland
- f* supported by the research grant No. 1 P03B 04529 (2005-2008)
- g* supported by the Polish National Science Centre, project No. DEC-2011/01/BST2/03643
- h* now at Rockefeller University, New York, NY 10065, USA
- i* now at DESY group FS-CFEL-1
- j* now at Institute of High Energy Physics, Beijing, China
- k* now at DESY group FEB, Hamburg, Germany
- l* also at Moscow State University, Russia
- m* now at University of Liverpool, United Kingdom
- n* now at CERN, Geneva, Switzerland
- o* also affiliated with Universtiy College London, UK
- p* now at Goldman Sachs, London, UK
- q* also at Institute of Theoretical and Experimental Physics, Moscow, Russia
- r* also at FPACS, AGH-UST, Cracow, Poland
- s* partially supported by Warsaw University, Poland
- t* now at Istituto Nucleare di Fisica Nazionale (INFN), Pisa, Italy
- u* now at Haase Energie Technik AG, Neumünster, Germany
- v* now at Department of Physics, University of Bonn, Germany
- w* also affiliated with DESY, Germany
- x* also at University of Tokyo, Japan
- y* now at Kobe University, Japan
- z* supported by DESY, Germany
- † deceased
- aa* member of National Technical University of Ukraine, Kyiv Polytechnic Institute, Kyiv, Ukraine
- ab* member of National University of Kyiv - Mohyla Academy, Kyiv, Ukraine
- ac* partly supported by the Russian Foundation for Basic Research, grant 11-02-91345-DFG_a
- ad* Alexander von Humboldt Professor; also at DESY and University of Oxford
- ae* STFC Advanced Fellow
- af* now at LNF, Frascati, Italy
- ag* This material was based on work supported by the National Science Foundation, while working at the Foundation.
- ah* also at Max Planck Institute for Physics, Munich, Germany, External Scientific Member
- ai* now at Tokyo Metropolitan University, Japan

- aj* now at Nihon Institute of Medical Science, Japan
- ak* now at Osaka University, Osaka, Japan
- al* also at Łódź University, Poland
- am* member of Łódź University, Poland
- an* now at Department of Physics, Stockholm University, Stockholm, Sweden
- ao* also at Cardinal Stefan Wyszyński University, Warsaw, Poland

1 Introduction

The study of deep inelastic scattering (DIS) of leptons off nucleons has contributed significantly to tests of the Standard Model (SM) of the electroweak and strong interactions. The structure of nucleons has mainly been determined from DIS experiments. The ep collider HERA has allowed an extension in the four-momentum-transfer squared, Q^2 , and in Bjorken x by several orders of magnitude with respect to previous fixed-target experiments [1]. The higher Q^2 reach of HERA has also allowed the exploration of the electroweak sector of the SM.

The ZEUS and H1 collaborations have both measured the e^-p and e^+p neutral current (NC) DIS cross sections up to Q^2 of 30 000 GeV² using the data collected in the years 1992–2000, referred to as the HERA I data-taking period. A combination of the results has been published [2].

The combined cross sections were used as the sole input to a next-to-leading order (NLO) QCD analysis to determine the set of parton distribution functions (PDFs) called HERAPDF1.0 [2]. The HERA I data were sufficiently precise to demonstrate the effects of Z exchange by comparing the e^-p and e^+p NC DIS cross sections at high Q^2 [2].

HERA underwent a major upgrade before the 2003–2007 data-taking period, referred to as HERA II running. The upgrade significantly increased the instantaneous luminosity delivered by HERA and also provided longitudinally polarised electron¹ beams for the collider experiments. The larger collected luminosity provided a higher reach in Q^2 and the longitudinal lepton-beam polarisation gave a unique opportunity to study the helicity structure of the electroweak interaction.

The ZEUS collaboration has already published the NC and CC inclusive cross sections for all HERA II running periods except for the NC e^+p data collected in 2006–2007 [3–6]. In this paper, we report NC e^+p cross sections for $Q^2 > 185$ GeV² for this period. The H1 collaboration has recently also published NC and CC cross sections for the HERA II running periods [7].

Parity-violating effects induced by electroweak processes can be demonstrated via the difference between the cross sections involving negatively and positively polarised electron beams. For positrons, this is expressed through the asymmetry parameter A^+ , which is proportional to the product of the electron axial (a_e) and quark vector (v_q) couplings to the Z boson. In this paper, the cross sections and the polarisation asymmetry are presented and compared to SM predictions, providing a test of the electroweak sector and a key input to further QCD fits.

¹ In this paper, the word “electron” refers to both electrons and positrons, unless otherwise stated.

2 Predictions from the Standard Model

Inclusive deep inelastic lepton-proton scattering can be described in terms of the kinematic variables x , y , and Q^2 . The variable Q^2 is defined as $Q^2 = -q^2 = -(k - k')^2$, where k and k' are the four-momenta of the incoming and scattered lepton, respectively. Bjorken x is defined as $x = Q^2/2P \cdot q$, where P is the four-momentum of the incoming proton. The fraction of the lepton energy transferred to the proton in the rest frame of the proton is given by $y = P \cdot q/P \cdot k$. The variables x , y and Q^2 are related by $Q^2 = sxy$, where s is the square of the lepton-proton centre-of-mass energy. At HERA, $s = 4E_e E_p$, where E_e and E_p are the initial electron and proton energies, respectively. The electroweak Born-level cross section for $e^\pm p$ NC interactions can be written as [8, 9]

$$\frac{d^2\sigma(e^\pm p)}{dx dQ^2} = \frac{2\pi\alpha^2}{xQ^4} [Y_+ \tilde{F}_2(x, Q^2) \mp Y_- x \tilde{F}_3(x, Q^2) - y^2 \tilde{F}_L(x, Q^2)], \quad (1)$$

where α is the fine-structure constant, $Y_\pm = 1 \pm (1 - y)^2$ and $\tilde{F}_2(x, Q^2)$, $\tilde{F}_3(x, Q^2)$ and $\tilde{F}_L(x, Q^2)$ are generalised structure functions. NLO QCD calculations predict [8, 9] and measurements confirm [10, 11] that the contribution of the longitudinal structure function, \tilde{F}_L , to $d^2\sigma/dx dQ^2$ is approximately 1%, averaged over the kinematic range considered here. However, in the high- y region, the \tilde{F}_L contribution to the cross section can be as large as 10% and it is therefore included in the SM predictions compared to the measurements presented in this paper.

The generalised structure functions depend on the longitudinal polarisation of the lepton beam, which is defined as

$$P_e = \frac{N_R - N_L}{N_R + N_L}, \quad (2)$$

where N_R and N_L are the numbers of right- and left-handed leptons in the beam².

The \tilde{F}_2 term in Eq. (1) is dominant at low Q^2 , where only photon exchange is important, while the \tilde{F}_3 term starts to contribute significantly to the cross section only at Q^2 values of the order of the mass of the Z boson squared, M_Z^2 , and above. It results from γ/Z interference and Z exchange. The sign of the \tilde{F}_3 term in Eq. (1) shows that electroweak effects decrease (increase) the e^+p (e^-p) cross section.

The reduced cross sections for e^-p and e^+p scattering are defined as

$$\tilde{\sigma}^{e^\pm p} = \frac{xQ^4}{2\pi\alpha^2} \frac{1}{Y_\pm} \frac{d^2\sigma(e^\pm p)}{dx dQ^2} = \tilde{F}_2(x, Q^2) \mp \frac{Y_-}{Y_+} x \tilde{F}_3(x, Q^2) - \frac{y^2}{Y_+} \tilde{F}_L(x, Q^2). \quad (3)$$

² At the HERA beam energies, the mass of the incoming leptons can be neglected, and therefore the difference between handedness and helicity can also be neglected.

Thus $x\tilde{F}_3$ can be obtained from the difference of the e^-p and e^+p reduced cross sections as

$$x\tilde{F}_3 = \frac{Y_+}{2Y_-}(\tilde{\sigma}^{e^-p} - \tilde{\sigma}^{e^+p}). \quad (4)$$

The generalised structure functions can be split into terms depending on γ exchange (F_2^γ), Z exchange (F_2^Z, xF_3^Z) and γ/Z interference ($F_2^{\gamma Z}, xF_3^{\gamma Z}$) as

$$\tilde{F}_2^\pm = F_2^\gamma - (v_e \pm P_e a_e)\chi_Z F_2^{\gamma Z} + (v_e^2 + a_e^2 \pm 2P_e v_e a_e)\chi_Z^2 F_2^Z, \quad (5)$$

$$x\tilde{F}_3^\pm = -(a_e \pm P_e v_e)\chi_Z xF_3^{\gamma Z} + (2v_e a_e \pm P_e(v_e^2 + a_e^2))\chi_Z^2 xF_3^Z. \quad (6)$$

The SM predictions for the respective vector and axial couplings of the electron to the Z boson are $v_e = -1/2 + 2\sin^2\theta_W$ and $a_e = -1/2$, where θ_W is the Weinberg angle. The relative fraction of events coming from Z with respect to γ exchange is given by

$$\chi_Z = \frac{1}{\sin^2 2\theta_W} \frac{Q^2}{M_Z^2 + Q^2}. \quad (7)$$

This fraction varies between 0.03 and 1.1 over the range of the analysis, $185 \text{ GeV}^2 < Q^2 < 50\,000 \text{ GeV}^2$. For the unpolarised case ($P_e = 0$), ignoring terms containing v_e , which is small (≈ -0.04), the interference structure function, $xF_3^{\gamma Z}$, is the dominant term in $x\tilde{F}_3$, and

$$x\tilde{F}_3 \simeq -a_e \chi_Z xF_3^{\gamma Z}. \quad (8)$$

The structure functions can be written in terms of the sum and differences of the quark and anti-quark momentum distributions. At leading order (LO) in QCD,

$$[F_2^\gamma, F_2^{\gamma Z}, F_2^Z] = \sum_q [e_q^2, 2e_q v_q, v_q^2 + a_q^2] x(q + \bar{q}), \quad (9)$$

$$[xF_3^{\gamma Z}, xF_3^Z] = \sum_q [e_q a_q, v_q a_q] 2x(q - \bar{q}), \quad (10)$$

where v_q and a_q are the respective vector and axial couplings of the quark q to the Z boson, and e_q is the electric charge of the quark. The densities of the quarks and anti-quarks are given by q and \bar{q} , respectively. The sum runs over all quark flavours except the top quark.

The sensitivity of $xF_3^{\gamma Z}$ to the u and d valence-quark momentum distributions is demonstrated in LO QCD through the expression

$$xF_3^{\gamma Z} = 2x[e_u a_u u_v + e_d a_d d_v] = \frac{x}{3}(2u_v + d_v), \quad (11)$$

where the SM values $v_u = 1/2 - 4/3\sin^2\theta_W$ and $a_u = 1/2$ have been used.

The charge-dependent polarisation asymmetry, A^+ , for a pure right-handed ($P_e = +1$) and left-handed ($P_e = -1$) positron beam is defined as

$$A^+ \equiv \frac{\sigma^+(P_e = +1) - \sigma^+(P_e = -1)}{\sigma^+(P_e = +1) + \sigma^+(P_e = -1)}, \quad (12)$$

where $\sigma^+(P_e = +1)$ and $\sigma^+(P_e = -1)$ are the differential e^+p cross sections evaluated at longitudinal polarisation values of +1 and -1, respectively. In general, A^+ can be calculated as

$$A^+ = \frac{\sigma^+(P_{e,+}) - \sigma^+(P_{e,-})}{P_{e,+}\sigma^+(P_{e,-}) - P_{e,-}\sigma^+(P_{e,+})}, \quad (13)$$

where $\sigma^+(P_{e,+})$ and $\sigma^+(P_{e,-})$ are the differential e^+p cross sections evaluated at any positive and negative polarisation values. For $P_{e,+} \approx -P_{e,-}$ this equation becomes

$$A^+ = \frac{2}{P_{e,+} - P_{e,-}} \cdot \frac{\sigma^+(P_{e,+}) - \sigma^+(P_{e,-})}{\sigma^+(P_{e,+}) + \sigma^+(P_{e,-})}. \quad (14)$$

Keeping only the leading terms, A^+ can be written as

$$A^+ \simeq -\chi_Z a_e \frac{F_2^{\gamma Z}}{F_2^\gamma} = -2\chi_Z a_e v_q e_q / e_q^2 \propto a_e v_q. \quad (15)$$

As the asymmetry parameter is proportional to the ratio of the $F_2^{\gamma Z}$ and F_2^γ structure functions, it is to first order insensitive to PDFs. Therefore a measurement of A^+ can give direct evidence of parity violation with minimal assumptions on the proton structure. As, in the SM, A^+ is expected to be a small quantity, less than 10% for Q^2 values below 2000 GeV², increasing slowly to 30% by Q^2 of 10 000 GeV², precise measurements of the polarised cross sections are required.

3 Experimental set-up

The analysis is based on a data sample collected in 2006–2007, when HERA collided positrons of energy $E_e = 27.5$ GeV with protons of energy $E_p = 920$ GeV, corresponding to a centre-of-mass energy $\sqrt{s} = 318$ GeV. The total integrated luminosity of the sample is 135.5 ± 2.5 pb⁻¹, of which 78.8 ± 1.4 pb⁻¹ were collected at a luminosity-weighted lepton-beam polarisation $P_e = 0.32 \pm 0.01$ and 56.7 ± 1.1 pb⁻¹ at $P_e = -0.36 \pm 0.01$.

A detailed description of the ZEUS detector can be found elsewhere [12]. A brief outline of the components that are most relevant for this analysis is given below.

Charged particles were tracked in the central tracking detector (CTD) [13] which operated in a magnetic field of 1.43 T provided by a thin superconducting solenoid. The CTD consisted of 72 cylindrical drift chamber layers, organised in nine superlayers covering the polar-angle³ region $15^\circ < \theta < 164^\circ$. The CTD was complemented by a silicon microvertex detector (MVD) [14], consisting of three active layers in the barrel and four disks in the forward region. For CTD-MVD tracks that pass through all nine CTD superlayers, the momentum resolution was $\sigma(p_T)/p_T = 0.0029p_T \oplus 0.0081 \oplus 0.0012/p_T$, with p_T in GeV.

The high-resolution uranium–scintillator calorimeter (CAL) [15] consisted of three parts: the forward (FCAL), the barrel (BCAL) and the rear (RCAL) calorimeters. Each part was subdivided transversely into towers and longitudinally into one electromagnetic section (EMC) and either one (in RCAL) or two (in BCAL and FCAL) hadronic sections (HAC). The smallest subdivision of the calorimeter is called a cell. The CAL energy resolutions, as measured under test-beam conditions, were $\sigma(E)/E = 0.18/\sqrt{E}$ for electrons and $\sigma(E)/E = 0.35/\sqrt{E}$ for hadrons, with E in GeV.

The luminosity was measured using the Bethe-Heitler reaction $ep \rightarrow e\gamma p$ by a luminosity detector which consisted of independent lead–scintillator calorimeter [16] and magnetic spectrometer [17] systems. The fractional systematic uncertainty on the measured luminosity was 1.8 % for the period with $P_e = 0.32$ and 1.9 % for the period with $P_e = -0.36$.

The lepton beam in HERA became naturally transversely polarised through the Sokolov-Ternov effect [18]. The characteristic build-up time in HERA was approximately 40 minutes. Spin rotators on either side of the ZEUS detector changed the transverse polarisation of the beam into longitudinal polarisation and back to transverse. The electron beam polarisation was measured using two independent polarimeters, the transverse polarimeter (TPOL) [19, 20] and the longitudinal polarimeter (LPOL) [21]. Both devices exploited the spin-dependent cross section for Compton scattering of circularly polarised photons off electrons to measure the beam polarisation. The luminosity and polarisation measurements were made over time scales that were much shorter than the polarisation build-up time.

³ The ZEUS coordinate system is a right-handed Cartesian system, with the Z axis pointing in the proton beam direction, referred to as the “forward direction”, and the X axis pointing towards the centre of HERA. The coordinate origin is at the nominal interaction point. The pseudorapidity is defined as $\eta = -\ln(\tan(\theta/2))$, where the polar angle, θ , is measured with respect to the proton beam direction.

4 Monte Carlo simulation

Monte Carlo (MC) simulations were used to determine the efficiency of the event selection, the accuracy of the kinematic reconstruction, to estimate the background rate and to extrapolate the measured cross sections to the full kinematic region. The effective luminosities of the MC samples were at least five times larger than that of the data sample and were normalised to the total integrated luminosity of the data.

Neutral current DIS events were simulated, including radiative effects, using the HERACLES [22] program with the DJANGO 1.6 [23] interface to the hadronisation programs and using the CTEQ5D [24] PDFs. The hadronic final state was simulated using the colour-dipole model of ARIADNE 4.12 [25]. To investigate systematic uncertainties, the MEPS model of LEPTO 6.5 [26] was also used. The Lund string model of JETSET 7.4 [27] was used for the hadronisation. Photoproduction (γp) events were simulated using HERWIG 5.9 [28] to study this background.

The ZEUS detector response was simulated using a program based on GEANT 3.21 [29]. The generated events were passed through the detector simulation, subjected to the same trigger requirements as the data and processed by the same reconstruction programs.

The distribution of the Z position of the interactions was a crucial input to the MC simulation with which the event-selection efficiency was determined. In order to measure this distribution, a special NC DIS sample was selected, for which the event selection efficiency did not depend on the Z of the interaction [30].

5 Event reconstruction

Neutral current events at high Q^2 are characterised by the presence of an isolated high-energy electron in the final state. The transverse momentum of the scattered electron balances that of the hadronic final state. Therefore the net transverse momentum of the event, P_T , representing the vectorial sum of the transverse momenta of all particles, \vec{p}_T , should be small. The measured net P_T and transverse energy, E_T , were calculated as

$$P_T^2 = P_X^2 + P_Y^2 = \left(\sum_i E_i \sin \theta_i \cos \phi_i \right)^2 + \left(\sum_i E_i \sin \theta_i \sin \phi_i \right)^2, \quad (16)$$
$$E_T = \sum_i E_i \sin \theta_i,$$

where the sum ran over all calorimeter energy deposits, E_i , and the polar (θ_i) and azimuthal (ϕ_i) angles were measured with respect to the interaction vertex. The variable δ ,

defined as

$$\delta \equiv \sum_i (E - P_Z)_i = \sum_i (E_i - E_i \cos \theta_i) \equiv E - P_Z, \quad (17)$$

was also used in the event selection. Conservation of energy and longitudinal momentum implies that $\delta = 2E_e = 55 \text{ GeV}$, if all final-state particles were detected and perfectly measured. Undetected particles that escape through the forward beam-hole had a negligible effect on δ . However, particles lost through the rear beam-hole could lead to a substantial reduction in δ . This was the case for γp events, where the electron emerged at a very small scattering angle, or for events in which an initial-state bremsstrahlung photon was emitted.

The CAL energy deposits were separated into those associated with the scattered electron and all other energy deposits. The sum of the latter was called the hadronic energy. The hadronic polar angle, γ_h , was defined as

$$\cos \gamma_h = \frac{P_{T,h}^2 - \delta_h^2}{P_{T,h}^2 + \delta_h^2}, \quad (18)$$

where the quantities $P_{T,h}$ and δ_h were derived from Eqs. (16–17) using only the hadronic energy. In the naïve quark-parton model, γ_h is the angle by which the struck quark is scattered.

The double angle (DA) method [31] used the polar angle of the scattered electron, θ_e , and the hadronic angle, γ_h , to reconstruct the kinematic variables x_{DA} , y_{DA} , and Q_{DA}^2 . For the determination of θ_e , tracking information was also used when available. The DA method was insensitive to uncertainties in the overall energy scale of the calorimeter. However, it was sensitive to initial-state QED radiation and an accurate simulation of the detector response was necessary. The variable y was reconstructed using the electron method (y_e). The Jacquet-Blondel method (y_{JB}) [32] was used in the event selection in kinematic regions where it provided better resolution.

6 Event selection

6.1 Trigger requirements

Events were selected using a three-level trigger system [12, 33, 34]. At the first level, only coarse calorimeter and tracking information was available. Events were selected if they had an energy deposit in the CAL consistent with an isolated electron. In addition, events with high E_T or high energy in the electromagnetic part of the calorimeter in coincidence with a CTD track were selected. At the second level, a requirement on δ

was used to select NC DIS events. Timing information from the calorimeter was used to reject events inconsistent with the bunch-crossing time. At the third level, events were fully reconstructed. The requirements were similar to, but looser than the offline cuts described below.

6.2 Offline requirements

The following criteria were imposed to select NC events.

- Electron identification:

an algorithm which combined information from the energy deposits in the calorimeter with tracks measured in the central tracking detectors was used to identify the scattered electron [35]. To ensure a high purity and to reject background, the identified electron was required to have an energy, E'_e , of at least 10 GeV and to be isolated such that the energy not associated with the electron in an $\eta - \phi$ cone of radius 0.8 centred on the electron was less than 5 GeV.

A track matched to the energy deposit in the calorimeter was required for events in which an electron was found within the region of good acceptance of the tracking detectors, which was $0.3 < \theta < 2.5$ [36]. This was done by restricting the distance of closest approach (DCA) between the track extrapolated to the calorimeter surface and the energy cluster position to within 10 cm and by requiring an electron track momentum (p_e^{trk}) larger than 3 GeV.

A matched track was not required if the electron emerged outside the acceptance of the tracking detectors.

- Background rejection:

the requirement $38 < \delta < 65$ GeV was imposed to remove γp and beam-gas events and to reduce the number of events with significant QED initial-state radiation. To further reduce background from γp events, y_e was required to be less than 0.9. The measured P_T was expected to be small for NC events. Therefore, in order to remove cosmic rays and beam-related background events, the quantity $P_T/\sqrt{E_T}$ was required to be less than $4\sqrt{\text{GeV}}$, and the quantity P_T/E_T was required to be less than 0.7.

- Additional requirements:

the projection of γ_h onto the face of FCAL was required to be outside a radius of 18 cm centred on the beam-pipe axis, to reject events where most of the hadronic final state was lost in the forward beam-pipe.

The Z coordinate of the ep interaction vertex, reconstructed using tracks in the CTD and the MVD, was required to satisfy $|Z_{\text{vtx}}| < 30$ cm.

In order to avoid the kinematic region in which the MC simulation is not appropriate due to missing higher-order QED corrections [23], the requirement $y_{\text{JB}}(1 - x_{\text{DA}})^2 > 0.004$ was applied.

The final event sample was selected by requiring $Q_{\text{DA}}^2 > 185 \text{ GeV}^2$.

A total of 302,073 candidate events passed the selection criteria. The background contamination estimated from the γp MC was about 0.2% overall.

Figure 1 shows a comparison between data and MC distributions for the variables Q_{DA}^2 , x_{DA} , y_{DA} , $E - P_Z$ of the event, θ_e and E'_e of the scattered electron and γ_h and $P_{T,h}$ of the final hadronic system. The description of the data by the MC is good.

7 Cross-section determination

The kinematic region of the measurement was defined as $Q^2 > 185 \text{ GeV}^2$, $y < 0.9$ and $y(1 - x)^2 > 0.004$. The single-differential cross-sections $d\sigma/dQ^2$, $d\sigma/dx$ and $d\sigma/dy$ and the reduced cross-section $\tilde{\sigma}^{e^+p}$ were measured. In addition, the single-differential cross-sections $d\sigma/dx$ and $d\sigma/dy$ were measured for the restricted range $Q^2 > 3000 \text{ GeV}^2$, $y < 0.9$ and $y(1 - x)^2 > 0.004$. The cross section in a particular bin ($d^2\sigma/dxdQ^2$ is used as an example) was determined according to

$$\frac{d^2\sigma}{dxdQ^2} = \frac{N_{\text{data}} - N_{\text{bg}}}{N_{\text{MC}}} \cdot \frac{d^2\sigma_{\text{Born}}^{\text{SM}}}{dxdQ^2}, \quad (19)$$

where N_{data} is the number of data events in the bin, N_{bg} is the number of background events predicted from the photoproduction MC and N_{MC} is the number of signal MC events normalised to the luminosity of the data. The SM prediction for the Born-level cross section, $d^2\sigma_{\text{Born}}^{\text{SM}}/dxdQ^2$, was evaluated using the CTEQ5D PDFs [24] as used for the MC simulation and using the PDG [37] values for the fine-structure constant, the mass of the Z boson and the weak mixing angle. This procedure implicitly takes into account the acceptance, bin-centering, and radiative corrections from the MC simulation. The bin sizes used for the determination of the single-differential and reduced cross sections were chosen to be commensurate with the detector resolutions. The statistical uncertainties on the cross sections were calculated from the number of events observed in the bins, taking into account the statistical uncertainty of the MC simulation (signal and background). Poisson statistics were used for all bins.

8 Systematic uncertainties

Systematic uncertainties were estimated [30, 36] by re-calculating the cross sections after modifying the analysis, in turn, for the uncertainties detailed below.

- δ_1 : the variation of the electron energy scale in the MC by its estimated uncertainty of $\pm 1\%$ resulted in changes of less than 0.5% in the cross sections over most of the kinematic region, due to the use of the DA reconstruction method. The effect was at most 3% in the high- y region of $d\sigma/dy$;
- δ_2 : the uncertainties due to “overlay” events, in which a DIS event overlapped with additional energy deposits from some other interaction in the RCAL, were estimated by narrowing or widening the $38 < \delta < 65$ GeV interval symmetrically by ± 2 GeV.⁴ The effect on the cross sections was typically below 1%. In a few high- Q^2 bins, the uncertainty was as large as 5%, reaching 11% in one reduced-cross-section bin;
- δ_3 : systematic uncertainties arising from the normalisation of the photoproduction background were determined by changing the background normalisation by its estimated uncertainty of $\pm 50\%$ [38]. The resulting changes in the cross sections were typically below 0.5%, reaching about 2% in the medium- Q^2 reduced-cross-section bins;
- δ_4 : to estimate the systematic uncertainty associated with the electron finder, an alternative electron-finding algorithm [39] was used and the results were compared to those obtained using the nominal algorithm. The systematic uncertainty from the electron-finding procedure was below 1% for most of the phase space;
- δ_5 : the upper limit of the θ range for which a matched track for the electron candidate was required was varied by ± 0.1 to account for uncertainties in the track-matching efficiency towards the edge of the CTD and BCAL. The uncertainty was mostly below 1.0%, but about 2% for the lower- Q^2 region;
- δ_6 : the systematic uncertainty due to the choice of the parton-shower scheme was evaluated by using the MEPS model of LEPTO to calculate the acceptance instead of ARIADNE⁵. The uncertainty was typically within 3%, but reached up to 8% in some bins of the reduced cross section and the highest bins of $d\sigma/dy$;
- δ_7 : the simulation of the first-level trigger was corrected in order to match the measured efficiency in the data. The systematic effect of the uncertainty of the correction on

⁴ This would also affect remaining photoproduction events. However, their contribution was negligible.

⁵ Since the simulation of the parton showers could, in principle, also have an influence on the electron isolation, the comparison was made removing the requirements on the electron isolation in order to prevent double counting of systematic uncertainty. However, no measurable influence of the isolation cut on δ_6 was observed.

the cross section was typically less than 1%, but reached about 2% for medium Q^2 and high y ;

- δ_8 : to evaluate the systematic uncertainty related to the electron isolation criterion, the isolation requirement was changed by ± 2 GeV from its nominal value of 5 GeV. The cross sections typically changed by much less than 0.5%;
- δ_9 : the DCA requirement was changed from 10 to 8 cm to estimate the uncertainty in the background contamination due to falsely identified electrons. The uncertainties in the cross sections associated with this variation were below 1% over most of the kinematic range;
- δ_{10} : the energy resolution used in the MC for the scattered electron was varied by its estimated uncertainty $\pm 1\%$. The effect on the cross sections was mostly less than 0.5% and less than 1% over the full kinematic range;
- δ_{11} : to account for differences of the p_e^{trk} distributions in data and MC, the p_e^{trk} requirement was varied by ± 1 GeV, resulting in a variation of the cross section by less than 0.5% over most of the kinematic range, and up to 6% in a few reduced-cross-section bins;
- δ_{12} : the cut of 18 cm on the projected radius of the hadronic angle onto the FCAL was varied by ± 2 cm. The cross sections typically changed by much less than 0.5%. The effect rises up to a maximum of 7% for the highest bins of both $d\sigma/dy$ and the reduced cross section;
- δ_{13} : the variation of the hadronic energy scale by its estimated uncertainty of $\pm 2\%$ in the MC resulted in changes of mostly below 0.5% and always less than 2% in the cross sections over the full kinematic range;
- δ_{14} : the systematic uncertainty associated with cosmic-ray rejection was evaluated by varying the $P_T/\sqrt{E_T}$ cut by $\pm 1\sqrt{\text{GeV}}$ and the P_T/E_T cut by ± 0.1 . The cross-section uncertainties were mostly below 0.5% reaching a maximum of 6% in one reduced-cross-section bin for the variation of the $p_T/\sqrt{E_T}$ cut;
- δ_{15} : The limit on the accepted $|Z_{\text{vtx}}|$ was varied by ± 5 cm, resulting in less than a 1% change in the cross sections over most of the kinematic range, reaching a maximum of 6% in the highest- Q^2 bins.

The 15 sources of systematic uncertainty were treated as uncorrelated to each other. Bin-to-bin correlations were found for δ 1,2,3,4,6,8,10,12 and 13. The positive and negative deviations from the nominal cross-section values were added in quadrature separately to obtain the total positive and negative systematic uncertainty.

The relative uncertainty in the measured polarisation was 4%. This has a negligible effect on the cross sections. The choice of which polarimeter to consider was made run-by-

run to maximise the available luminosity and minimise the uncertainty in the measured polarisation.

The measured luminosity had a relative uncertainty of 1.8% for the period with right-handed and 1.9% for the period with left-handed polarisation. The uncertainties in the luminosity and polarisation measurements were not included in the total systematic uncertainty shown in the final results.

9 Results

9.1 Unpolarised cross sections

The single-differential cross sections as a function of Q^2 , x and y , extracted using the full data sample, are shown in Figs. 2–4 and tabulated in Tables 1–3. In all tables, the total systematic uncertainty as described in Section 8 is given. The numbers for the individual contributions are available electronically [40, 41].

Combining the data from the negatively and positively polarised beams resulted in a residual polarisation of 0.03 which was corrected for using theoretical predictions in NLO QCD with electroweak corrections.

The measurement of $d\sigma/dQ^2$, shown in Fig. 2, falls over seven orders of magnitude in the measured range covering two orders of magnitude in Q^2 . In this figure, the ratio of the measured cross sections and the SM predictions evaluated using the HERAPDF1.5 PDFs [42, 43] and the PDFs from ZEUSJETS [44], CTEQ6M [45] and MSTW2008 [46] are shown. The SM predictions differ depending on the PDFs. Taking into account the luminosity uncertainty, which is not shown in the figures, the data are well described by the SM predictions. The cross-sections $d\sigma/dx$ and $d\sigma/dy$ are shown in Fig. 3 and Fig. 4 for the nominal range, $Q^2 > 185 \text{ GeV}^2$, and for $Q^2 > 3000 \text{ GeV}^2$. The figures demonstrate the precision of this measurement. The measured cross sections are well described by the SM prediction evaluated using the HERAPDF1.5 PDFs.⁶

The reduced cross sections of unpolarised e^+p NC DIS, tabulated in Table 4, are shown in Fig. 5. The residual polarisation was corrected for using theoretical predictions. The SM predictions are in good agreement with the measurements over the full kinematic range. Also shown are the unpolarised e^-p NC DIS cross sections, measured using an integrated luminosity of 169.9 pb^{-1} collected between 2005 and 2006 [5]. In Section 2, it was discussed that the e^-p and e^+p reduced cross sections only differ at high Q^2 . As the

⁶ HERAPDF1.5 is based on HERA I and HERA II data, but the data presented here is not used for the extraction.

contribution of $x\tilde{F}_3$ has to be extracted through a subtraction (see Eq. (4)), a very precise measurement of these cross sections is needed.

Figure 6 shows the result on $x\tilde{F}_3$ obtained according to Eq. (4) from the unpolarised e^+p and e^-p reduced cross sections in the high- Q^2 region. The systematic uncertainties were treated as uncorrelated between the e^+p and the e^-p measurements in the extraction of $x\tilde{F}_3$. The measurements are well described by the SM predictions. The results are also given in Table 5.

The structure-function $xF_3^{\gamma Z}$ has little dependence on Q^2 . Therefore a higher statistical significance could be obtained by averaging the measurements after an extrapolation to $1\,500\text{ GeV}^2$. The structure-function $xF_3^{\gamma Z}$ measured at $Q^2 = 1\,500\text{ GeV}^2$, tabulated in Table 6, is shown in Fig. 7. It is well described by the SM predictions.

The inclusive cross sections presented here provide valuable information to the global fits [46, 47] for parton distribution functions over a wide range of Bjorken x values from $\sim 10^{-2}$ to 0.65.

9.2 Polarised cross sections

The effects of the longitudinal polarisation of the electrons becomes significant at the electroweak scale, where the contributions of both γ and Z exchange to the cross section are comparable. The reduced cross sections for positive and negative longitudinal polarisations, tabulated in Tables 7 to 8, are shown in Fig. 8. The data are also well described by the SM predictions using the HERAPDF1.5 PDFs. At high Q^2 , a difference between the positively and negatively polarised cross sections is predicted. To demonstrate this effect, the single-differential cross-section $d\sigma/dQ^2$ was measured separately for positive and negative beam polarisations. The results are shown in Fig. 9. Both measurements are well described by the SM predictions using different sets of PDFs taking the uncertainty due to the luminosity measurement into account. The single-differential cross sections as a function of Q^2 , x and y , extracted using the negatively and positively polarised data samples separately, are tabulated in Tables 9 to 14.

The ratio of the measured single-differential cross-section $d\sigma/dQ^2$ for the two different polarisation states is shown in Fig. 10 (a). The difference between the two polarisation states is clearly visible at higher Q^2 . The asymmetry A^+ (see Eq. (13)) extracted from these measurements is tabulated in Table 15 and is shown in Fig. 10 (b), where only statistical uncertainties are considered. The uncertainty in A^+ arising from the relative normalization between the data sets was evaluated to be 1%. The other systematic uncertainties are assumed to cancel. The SM also describes these results well. The deviation of A^+ from zero, particularly at high Q^2 , shows the difference in the behaviour

of the two polarisation states and is clear evidence of parity violation. The precision of the data makes the effect also clearly visible at relatively low Q^2 , where it is intrinsically small.

The effect of γ/Z interference is quantified by calculating the χ^2 per degree of freedom of A^+ with respect both to zero and to the SM prediction using the HERAPDF1.5 PDFs. The $\chi^2/\text{d.o.f.}$ with respect to zero is determined to be 9.0, whereas the $\chi^2/\text{d.o.f.}$ with respect to the SM prediction is 1.5. Thus parity violation in ep NC DIS is demonstrated at scales down to $\approx 10^{-18}$ m.

The polarised cross sections presented here constrain the vector couplings of the quarks to the Z (see Eq. (15)) when included in the PDF fits. Therefore, this measurement is a stringent test of the electroweak sector of the Standard Model. The data can also be used to test physics beyond the Standard Model like setting limits on the production of leptoquarks [48].

10 Conclusions

The cross sections for neutral current deep inelastic e^+p scattering with a longitudinally polarised positron beam have been measured. The measurements are based on a data sample corresponding to an integrated luminosity of 135.5 pb^{-1} collected with the ZEUS detector at HERA from 2006 to 2007 at a centre-of-mass energy of 318 GeV. The accessible range in Q^2 extended to $Q^2 = 50\,000 \text{ GeV}^2$, allowing for a stringent test of electroweak effects in the Standard Model.

The single-differential cross sections as a function of Q^2 , x and y were presented for $Q^2 > 185 \text{ GeV}^2$, $y < 0.9$ and $y(1-x)^2 > 0.004$, where the data obtained with negatively and positively polarised beams were combined. The cross-sections $d\sigma/dx$ and $d\sigma/dy$ were also measured for $Q^2 > 3\,000 \text{ GeV}^2$, $y < 0.9$ and $y(1-x)^2 > 0.004$. The reduced cross section was measured at zero polarisation by correcting for the residual polarisation of the combined data sample. These measurements were combined with previously measured e^-p neutral current cross sections to extract $x\tilde{F}_3$. In addition, the interference structure function $xF_3^{\gamma Z}$ was extracted at an average value of $Q^2 = 1\,500 \text{ GeV}^2$.

The reduced cross section and the single-differential cross-sections $d\sigma/dQ^2$, $d\sigma/dx$ and $d\sigma/dy$ were also measured separately for positive and negative values of the longitudinal polarisation of the positron beam. Parity violation was observed through the polarisation asymmetry A^+ . The measured cross sections confirm the predictions of the Standard Model and provide strong constraints at the electroweak scale.

Acknowledgements

We appreciate the contributions to the construction and maintenance of the ZEUS detector of many people who are not listed as authors. The HERA machine group and the DESY computing staff are especially acknowledged for their success in providing excellent operation of the collider and the data-analysis environment. We thank the DESY directorate for their strong support and encouragement.

References

- [1] H. Abramowicz and A. Caldwell, *Rev. Mod. Phys.* 71 (1999) 1275.
- [2] H1 Collaboration and ZEUS Collaboration, F.D. Aaron et al., *JHEP* 01 (2010) 109.
- [3] ZEUS Collaboration, S. Chekanov et al., *Phys. Lett. B* 637 (2006) 210.
- [4] ZEUS Collaboration, S. Chekanov et al., *Eur. Phys. J. C* 61 (2009) 223.
- [5] ZEUS Collaboration, S. Chekanov et al., *Eur. Phys. J. C* 62 (2009) 625.
- [6] ZEUS Collaboration, S. Chekanov et al., *Eur. Phys. J. C* 70 (2010) 945.
- [7] H1 Collaboration, A. Aktas et al., Preprint hep-ex/1206.7007, 2012.
- [8] R. Devenish and A. Cooper-Sarkar, *Deep Inelastic Scattering*. Oxford University Press, 2003.
- [9] M. Klein and T. Riemann, *Z. Phys. C* 24 (1984) 151.
- [10] ZEUS Collaboration, S. Chekanov et al., *Phys. Lett. B* 682 (2009) 8.
- [11] H1 Collaboration, A. Aktas et al., *Eur. Phys. J. C* 71 (2011) 1579.
- [12] ZEUS Collaboration, U. Holm (ed.), *The ZEUS Detector*. Status Report (unpublished), DESY (1993), available on <http://www-zeus.desy.de/bluebook/bluebook.html>.
- [13] N. Harnew et al., *Nucl. Inst. Meth. A* 279 (1989) 290;
B. Foster et al., *Nucl. Phys. Proc. Suppl. B* 32 (1993) 181;
B. Foster et al., *Nucl. Inst. Meth. A* 338 (1994) 254.
- [14] A. Polini et al., *Nucl. Inst. Meth. A* 581 (2007) 656.
- [15] M. Derrick et al., *Nucl. Inst. Meth. A* 309 (1991) 77;
A. Andresen et al., *Nucl. Inst. Meth. A* 309 (1991) 101;
A. Caldwell et al., *Nucl. Inst. Meth. A* 321 (1992) 356;
A. Bernstein et al., *Nucl. Inst. Meth. A* 336 (1993) 23.
- [16] J. Andruszków et al., Preprint DESY-92-066, DESY, 1992;
ZEUS Collaboration, M. Derrick et al., *Z. Phys. C* 63 (1994) 391;
J. Andruszków et al., *Acta Phys. Pol. B* 32 (2001) 2025.
- [17] M. Helbich et al., Preprint physics/0512153, 2005. Submitted to *Nucl. Inst. Meth.*
- [18] A.A. Sokolov and I.M. Ternov, *Sov. Phys. Dokl.* 8 (1964) 1203.
- [19] V.N. Baier and V.A. Khoze, *Sov. J. Nucl. Phys.* 9 (1969) 238.
- [20] D.P. Barber et al., *Nucl. Inst. Meth. A* 329 (1993) 79.
- [21] M. Beckmann et al., *Nucl. Inst. Meth. A* 479 (2002) 334.

- [22] A. Kwiatkowski, H. Spiesberger and H.-J. Möhring, *Comp. Phys. Comm.* 69 (1992) 155. Also in *Proc. Workshop Physics at HERA*, eds. W. Buchmüller and G. Ingelman, (DESY, Hamburg, 1991).
- [23] G.A. Schuler and H. Spiesberger, *Proc. Workshop on Physics at HERA*, W. Buchmüller and G. Ingelman (eds.), Vol. 3, p. 1419. Hamburg, Germany, DESY (1991);
H. Spiesberger, *HERACLES and DJANGO: Event Generation for ep Interactions at HERA Including Radiative Processes*, 1998, available on <http://www.desy.de/~hspiesb/djangoh.html>.
- [24] CTEQ Collaboration, H.L. Lai et al., *Eur. Phys. J. C* 12 (2000) 375.
- [25] L. Lönnblad, *Comp. Phys. Comm.* 71 (1992) 15.
- [26] A. Edin, G. Ingelman and J. Rathsman, *Phys. Lett. B* 366 (1996) 371.
- [27] T. Sjöstrand, *Comp. Phys. Comm.* 39 (1986) 347;
T. Sjöstrand and M. Bengtsson, *Comp. Phys. Comm.* 43 (1987) 367;
T. Sjöstrand, *Comp. Phys. Comm.* 82 (1994) 74.
- [28] G. Marchesini et al., *Comp. Phys. Comm.* 67 (1992) 465.
- [29] R. Brun et al., GEANT3, Technical Report CERN-DD/EE/84-1, CERN, 1987.
- [30] T. Stewart. Ph.D. Thesis, University of Toronto, Report DESY-THESIS-2012-028, 2012, available on <http://www-library.desy.de/cgi-bin/showprep.pl?desy-thesis-12-028&relax> .
- [31] S. Bentvelsen, J. Engelen and P. Kooijman, *Proc. Workshop on Physics at HERA*, W. Buchmüller and G. Ingelman (eds.), Vol. 1, p. 23. Hamburg, Germany, DESY (1992);
K.C. Höger, *Proc. Workshop on Physics at HERA*, W. Buchmüller and G. Ingelman (eds.), Vol. 1, p. 43. Hamburg, Germany, DESY (1992).
- [32] F. Jacquet and A. Blondel, *Proceedings of the Study for an ep Facility for Europe*, U. Amaldi (ed.), p. 391. Hamburg, Germany (1979). Also in preprint DESY 79/48.
- [33] W.H. Smith, K. Tokushuku and L.W. Wiggers, *Proc. Computing in High-Energy Physics (CHEP), Annecy, France, Sept. 1992*, C. Verkerk and W. Wojcik (eds.), p. 222. CERN, Geneva, Switzerland (1992). Also in preprint DESY 92-150B.
- [34] P.D. Allfrey et al., *Nucl. Inst. Meth. A* 580 (2007) 1257.
- [35] ZEUS Collaboration, J. Breitweg et al., *Eur. Phys. J. C* 11 (1999) 427.
- [36] F. Januschek. Ph.D. Thesis, University of Hamburg, Report DESY-THESIS-2012-012, 2012, available on <http://www-library.desy.de/cgi-bin/showprep.pl?desy-thesis-12-012&relax> .

- [37] Particle Data Group, D.E. Groom et al., *Eur. Phys. J. C* 15 (2000) 1.
- [38] M. Wlasenko. Ph.D. Thesis, University of Bonn, Report BONN-IR-2009-05, 2009, available on <http://inspirehep.net/record/867159/files/867159.pdf>.
- [39] H. Abramowicz, A. Caldwell and R. Sinkus, *Nucl. Inst. Meth. A* 365 (1995) 508.
- [40] ZEUS Collaboration, *ZEUS database*, 2012, available on http://www-zeus.desy.de/zeus_papers/zeus_papers.html#12-145.
- [41] Durham University, *The Durham HepData Project*, 2012, available on <http://hepdata.cedar.ac.uk/>.
- [42] H1 Collaboration and ZEUS Collaboration, H. Abramowicz et al., *QCD NLO analysis of inclusive data (HERAPDF 1.5)* (unpublished), 2010, available on https://www.desy.de/h1zeus/combined_results/herapdf/table/. H1prelim-10-142, ZEUS-prel-10-018.
- [43] V. Radescu, *Proceedings of the 35th International Conference on High Energy Physics, ICHEP 2010, Paris, France, July 22-28, 2010*, B. Pire et al. (ed.), Vol. ICHEP2010, p. 168. (2010).
- [44] ZEUS Collaboration, S. Chekanov et al., *Eur. Phys. J. C* 42 (2005) 1.
- [45] J. Pumplin et al., *JHEP* 07 (2002) 012.
- [46] A.D. Martin et al., *Eur. Phys. J. C* 63 (2009) 189.
- [47] P.M. Nadolsky et al., *Phys. Rev. D* 78 (2008) 013004.
- [48] ZEUS Collaboration, H. Abramovic et al., *Phys. Rev. D* 86 (2012) 012005.

Q^2 range (GeV ²)	Q_c^2 (GeV ²)	$d\sigma/dQ^2$ (pb/GeV ²)	N_{data}	$N_{\text{bg}}^{\text{MC}}$
185 – 210	195	$(1.91 \pm 0.01^{+0.02}_{-0.01}) \times 10^1$	55281	110.1
210 – 240	220	$(1.43 \pm 0.01^{+0.01}_{-0.01}) \times 10^1$	47861	73.8
240 – 270	255	$(1.01 \pm 0.01^{+0.01}_{-0.01}) \times 10^1$	34808	59.2
270 – 300	285	$(7.79 \pm 0.05^{+0.07}_{-0.09})$	25835	18.9
300 – 340	320	$(5.79 \pm 0.04^{+0.09}_{-0.05})$	24184	32.8
340 – 380	360	$(4.35 \pm 0.03^{+0.07}_{-0.02})$	17201	22.8
380 – 430	400	$(3.33 \pm 0.03^{+0.06}_{-0.03})$	15791	28.5
430 – 480	450	$(2.56 \pm 0.02^{+0.05}_{-0.05})$	11903	40.1
480 – 540	510	$(1.89 \pm 0.02^{+0.02}_{-0.05})$	10365	19.9
540 – 600	570	$(1.39 \pm 0.02^{+0.03}_{-0.03})$	6943	36.2
600 – 670	630	$(1.14 \pm 0.01^{+0.02}_{-0.03})$	6366	20.1
670 – 740	700	$(8.70 \pm 0.12^{+0.19}_{-0.29}) \times 10^{-1}$	5655	22.5
740 – 820	780	$(6.65 \pm 0.09^{+0.09}_{-0.19}) \times 10^{-1}$	5750	16.9
820 – 900	860	$(5.08 \pm 0.07^{+0.09}_{-0.17}) \times 10^{-1}$	4654	25.0
900 – 990	940	$(4.16 \pm 0.06^{+0.06}_{-0.14}) \times 10^{-1}$	4295	15.6
990 – 1080	1030	$(3.20 \pm 0.06^{+0.09}_{-0.13}) \times 10^{-1}$	3304	10.5
1080 – 1200	1130	$(2.55 \pm 0.04^{+0.04}_{-0.06}) \times 10^{-1}$	3522	18.1
1200 – 1350	1270	$(1.96 \pm 0.03^{+0.06}_{-0.05}) \times 10^{-1}$	3439	14.6
1350 – 1500	1420	$(1.42 \pm 0.03^{+0.03}_{-0.03}) \times 10^{-1}$	2501	16.4
1500 – 1700	1590	$(1.08 \pm 0.02^{+0.03}_{-0.02}) \times 10^{-1}$	2549	8.3
1700 – 1900	1790	$(7.84 \pm 0.18^{+0.21}_{-0.13}) \times 10^{-2}$	1849	8.5
1900 – 2100	1990	$(5.88 \pm 0.16^{+0.21}_{-0.10}) \times 10^{-2}$	1393	9.1
2100 – 2600	2300	$(4.02 \pm 0.08^{+0.08}_{-0.08}) \times 10^{-2}$	2311	7.2
2600 – 3200	2800	$(2.34 \pm 0.06^{+0.03}_{-0.04}) \times 10^{-2}$	1565	3.3
3200 – 3900	3500	$(1.31 \pm 0.04^{+0.03}_{-0.03}) \times 10^{-2}$	1083	1.1
3900 – 4700	4200	$(7.77 \pm 0.29^{+0.14}_{-0.14}) \times 10^{-3}$	715	3.9
4700 – 5600	5100	$(4.18 \pm 0.20^{+0.04}_{-0.12}) \times 10^{-3}$	447	0.0
5600 – 6600	6050	$(2.66 \pm 0.15^{+0.03}_{-0.06}) \times 10^{-3}$	320	0.0
6600 – 7800	7100	$(1.47 \pm 0.10^{+0.04}_{-0.06}) \times 10^{-3}$	208	0.0
7800 – 9200	8400	$(9.20 \pm 0.74^{+0.31}_{-0.34}) \times 10^{-4}$	152	0.0
9200 – 12800	10800	$(3.40 \pm 0.28^{+0.09}_{-0.10}) \times 10^{-4}$	145	0.0
12800 – 18100	15200	$(9.21 \pm 1.21^{+0.31}_{-0.76}) \times 10^{-5}$	57	0.0
18100 – 25600	21500	$(3.81^{+0.76}_{-0.64} \pm 0.23^{+0.23}_{-0.23}) \times 10^{-5}$	35	0.0
25600 – 50000	36200	$(8.23^{+6.51}_{-3.94} \pm 0.71^{+0.71}_{-0.44}) \times 10^{-7}$	4	0.0

Table 1: The single-differential cross-section $d\sigma/dQ^2$ ($y < 0.9$, $y(1-x)^2 > 0.004$) for the reaction $e^+p \rightarrow e^+X$ ($\mathcal{L} = 135.5 \text{ pb}^{-1}$, corrected to $P_e = 0$). The bin range, bin centre (Q_c^2) and measured cross section corrected to the electroweak Born level are shown. The first (second) error on the cross section corresponds to the statistical (systematic) uncertainties. The number of observed data events (N_{data}) and simulated background events ($N_{\text{bg}}^{\text{MC}}$) are also shown.

$Q^2 >$ (GeV ²)	x range	x_c	$d\sigma/dx$ (pb)	N_{data}	$N_{\text{bg}}^{\text{MC}}$
185	$(0.63 - 1.00) \times 10^{-2}$	0.794×10^{-2}	$(8.71 \pm 0.05^{+0.13}_{-0.14}) \times 10^4$	34570	161.0
	$(0.10 - 0.16) \times 10^{-1}$	0.126×10^{-1}	$(5.84 \pm 0.03^{+0.07}_{-0.17}) \times 10^4$	39862	122.5
	$(0.16 - 0.25) \times 10^{-1}$	0.200×10^{-1}	$(3.63 \pm 0.02^{+0.03}_{-0.03}) \times 10^4$	39233	82.9
	$(0.25 - 0.40) \times 10^{-1}$	0.316×10^{-1}	$(2.10 \pm 0.01^{+0.02}_{-0.01}) \times 10^4$	38384	30.2
	$(0.40 - 0.63) \times 10^{-1}$	0.501×10^{-1}	$(1.24 \pm 0.01^{+0.01}_{-0.01}) \times 10^4$	33557	5.5
	$(0.63 - 1.00) \times 10^{-1}$	0.794×10^{-1}	$(6.90 \pm 0.04^{+0.08}_{-0.03}) \times 10^3$	31825	5.1
	0.10 - 0.16	0.126	$(3.89 \pm 0.02^{+0.04}_{-0.02}) \times 10^3$	30244	1.4
	0.16 - 0.25	0.200	$(2.04 \pm 0.01^{+0.04}_{-0.06}) \times 10^3$	18768	0.0
3000	$(0.40 - 0.63) \times 10^{-1}$	0.501×10^{-1}	$(1.71 \pm 0.08^{+0.06}_{-0.03}) \times 10^2$	440	1.1
	$(0.63 - 1.00) \times 10^{-1}$	0.794×10^{-1}	$(1.60 \pm 0.06^{+0.04}_{-0.02}) \times 10^2$	714	3.9
	0.10 - 0.16	0.126	$(1.18 \pm 0.04^{+0.01}_{-0.04}) \times 10^2$	859	0.0
	0.16 - 0.25	0.200	$(6.72 \pm 0.25^{+0.06}_{-0.16}) \times 10^1$	730	0.0
	0.25 - 0.40	0.316	$(3.22 \pm 0.14^{+0.04}_{-0.08}) \times 10^1$	567	0.0
	0.40 - 0.75	0.687	$(1.20 \pm 0.08^{+0.02}_{-0.02})$	240	0.0

Table 2: The single-differential cross-section $d\sigma/dx$ ($y < 0.9$, $y(1-x)^2 > 0.004$) for $Q^2 > 185 \text{ GeV}^2$ and $Q^2 > 3000 \text{ GeV}^2$ for the reaction $e^+p \rightarrow e^+X$ ($\mathcal{L} = 135.5 \text{ pb}^{-1}$, corrected to $P_e = 0$). The Q^2 and bin range, bin centre (x_c) and measured cross section corrected to the electroweak Born level are shown. Other details as in Table 1.

$Q^2 >$ (GeV ²)	y range	y_c	$d\sigma/dy$ (pb)	N_{data}	$N_{\text{bg}}^{\text{MC}}$
185	0.00 – 0.05	0.025	$(1.63 \pm 0.01_{-0.01}^{+0.02}) \times 10^4$	75314	0.0
	0.05 – 0.10	0.075	$(8.10 \pm 0.04_{-0.05}^{+0.09}) \times 10^3$	50532	7.4
	0.10 – 0.15	0.125	$(5.64 \pm 0.03_{-0.05}^{+0.03}) \times 10^3$	34944	11.6
	0.15 – 0.20	0.175	$(4.37 \pm 0.03_{-0.14}^{+0.02}) \times 10^3$	26237	24.7
	0.20 – 0.25	0.225	$(3.61 \pm 0.03_{-0.20}^{+0.03}) \times 10^3$	20974	19.8
	0.25 – 0.30	0.275	$(2.93 \pm 0.02_{-0.04}^{+0.04}) \times 10^3$	16254	17.7
	0.30 – 0.35	0.325	$(2.53 \pm 0.02_{-0.03}^{+0.04}) \times 10^3$	13919	44.6
	0.35 – 0.40	0.375	$(2.24 \pm 0.02_{-0.03}^{+0.02}) \times 10^3$	12202	43.8
	0.40 – 0.45	0.425	$(1.98 \pm 0.02_{-0.02}^{+0.03}) \times 10^3$	10402	62.6
	0.45 – 0.50	0.475	$(1.73 \pm 0.02_{-0.01}^{+0.05}) \times 10^3$	8761	50.6
	0.50 – 0.55	0.525	$(1.54 \pm 0.02_{-0.01}^{+0.04}) \times 10^3$	7661	54.4
	0.55 – 0.60	0.575	$(1.42 \pm 0.02_{-0.03}^{+0.04}) \times 10^3$	6794	64.1
	0.60 – 0.65	0.625	$(1.29 \pm 0.02_{-0.04}^{+0.04}) \times 10^3$	5723	63.0
	0.65 – 0.70	0.675	$(1.21 \pm 0.02_{-0.05}^{+0.04}) \times 10^3$	4671	25.1
	0.70 – 0.75	0.725	$(1.12 \pm 0.02_{-0.05}^{+0.07}) \times 10^3$	3542	48.3
	0.75 – 0.90	0.825	$(9.54 \pm 0.14_{-0.46}^{+0.76}) \times 10^2$	4433	103.8
3000	0.05 – 0.10	0.075	$(3.27 \pm 0.25_{-0.03}^{+0.06}) \times 10^1$	174	0.0
	0.10 – 0.15	0.125	$(5.56 \pm 0.31_{-0.13}^{+0.05}) \times 10^1$	326	0.0
	0.15 – 0.20	0.175	$(5.91 \pm 0.31_{-0.08}^{+0.07}) \times 10^1$	357	0.0
	0.20 – 0.25	0.225	$(5.62 \pm 0.30_{-0.20}^{+0.05}) \times 10^1$	345	0.0
	0.25 – 0.30	0.275	$(4.97 \pm 0.28_{-0.18}^{+0.04}) \times 10^1$	312	0.0
	0.30 – 0.35	0.325	$(5.13 \pm 0.29_{-0.13}^{+0.05}) \times 10^1$	321	0.0
	0.35 – 0.40	0.375	$(3.72 \pm 0.24_{-0.20}^{+0.04}) \times 10^1$	233	0.0
	0.40 – 0.45	0.425	$(3.40 \pm 0.23_{-0.12}^{+0.04}) \times 10^1$	214	0.0
	0.45 – 0.50	0.475	$(3.59 \pm 0.24_{-0.08}^{+0.04}) \times 10^1$	224	0.0
	0.50 – 0.55	0.525	$(2.82 \pm 0.21_{-0.08}^{+0.04}) \times 10^1$	173	0.0
	0.55 – 0.60	0.575	$(2.94 \pm 0.22_{-0.04}^{+0.03}) \times 10^1$	178	0.0
	0.60 – 0.65	0.625	$(2.41 \pm 0.20_{-0.04}^{+0.14}) \times 10^1$	152	3.9
	0.65 – 0.70	0.675	$(2.27 \pm 0.20_{-0.10}^{+0.05}) \times 10^1$	134	0.0
	0.70 – 0.75	0.725	$(2.35 \pm 0.20_{-0.13}^{+0.05}) \times 10^1$	134	0.0
	0.75 – 0.80	0.775	$(2.10 \pm 0.19_{-0.12}^{+0.14}) \times 10^1$	119	0.0
	0.80 – 0.85	0.825	$(1.89 \pm 0.19_{-0.05}^{+0.26}) \times 10^1$	103	1.1
0.85 – 0.90	0.875	$(1.92 \pm 0.21_{-0.16}^{+0.20}) \times 10^1$	87	0.0	

Table 3: The single-differential cross-section $d\sigma/dy$ for $Q^2 > 185 \text{ GeV}^2$ and $Q^2 > 3000 \text{ GeV}^2$ ($y(1-x)^2 > 0.004$) for the reaction $e^+p \rightarrow e^-X$ ($\mathcal{L} = 135.5 \text{ pb}^{-1}$, corrected to $P_e = 0$). The Q^2 and bin range, bin centre (y_c) and measured cross section corrected to the electroweak Born level are shown. Other details as in Table 1.

Q^2 range (GeV ²)	Q_c^2 (GeV ²)	x range	x_c	$\tilde{\sigma}$	N_{data}	$N_{\text{bg}}^{\text{MC}}$
185 – 240	200	0.004 – 0.006	0.005	$(1.110 \pm 0.010^{+0.029}_{-0.017})$	13313	108.0
	200	0.006 – 0.010	0.008	$(0.945 \pm 0.008^{+0.008}_{-0.022})$	15647	38.8
	200	0.010 – 0.017	0.013	$(0.801 \pm 0.006^{+0.002}_{-0.022})$	16074	14.1
	200	0.017 – 0.025	0.021	$(0.680 \pm 0.006^{+0.013}_{-0.004})$	11107	5.1
	200	0.025 – 0.037	0.032	$(0.566 \pm 0.006^{+0.015}_{-0.001})$	9767	0.0
	200	0.037 – 0.060	0.050	$(0.511 \pm 0.005^{+0.011}_{-0.002})$	10375	1.1
	200	0.060 – 0.120	0.080	$(0.433 \pm 0.004^{+0.016}_{-0.001})$	13867	0.0
240 – 310	200	0.120 – 0.250	0.180	$(0.346 \pm 0.004^{+0.006}_{-0.008})$	8823	0.0
	250	0.006 – 0.010	0.008	$(0.929 \pm 0.010^{+0.022}_{-0.011})$	9190	34.9
	250	0.010 – 0.017	0.013	$(0.821 \pm 0.008^{+0.006}_{-0.035})$	10611	10.0
	250	0.017 – 0.025	0.021	$(0.692 \pm 0.008^{+0.005}_{-0.008})$	7770	6.4
	250	0.025 – 0.037	0.032	$(0.585 \pm 0.007^{+0.012}_{-0.011})$	7466	1.1
	250	0.037 – 0.060	0.050	$(0.513 \pm 0.006^{+0.012}_{-0.008})$	7740	0.0
	250	0.060 – 0.120	0.080	$(0.435 \pm 0.004^{+0.010}_{-0.005})$	10142	0.0
310 – 410	250	0.120 – 0.250	0.180	$(0.337 \pm 0.004^{+0.005}_{-0.008})$	8042	0.0
	350	0.006 – 0.010	0.008	$(0.948 \pm 0.013^{+0.033}_{-0.008})$	5579	27.3
	350	0.010 – 0.017	0.013	$(0.809 \pm 0.010^{+0.009}_{-0.019})$	7000	6.1
	350	0.017 – 0.025	0.021	$(0.673 \pm 0.009^{+0.009}_{-0.010})$	5167	0.9
	350	0.025 – 0.037	0.032	$(0.575 \pm 0.008^{+0.017}_{-0.004})$	4869	1.1
	350	0.037 – 0.060	0.050	$(0.507 \pm 0.007^{+0.011}_{-0.005})$	5306	1.1
	350	0.060 – 0.120	0.080	$(0.418 \pm 0.005^{+0.016}_{-0.004})$	6823	0.0
410 – 530	350	0.120 – 0.250	0.180	$(0.325 \pm 0.004^{+0.007}_{-0.005})$	6340	0.0
	450	0.006 – 0.010	0.008	$(1.023 \pm 0.015^{+0.019}_{-0.020})$	4548	44.9
	450	0.010 – 0.017	0.013	$(0.816 \pm 0.014^{+0.010}_{-0.018})$	3304	6.8
	450	0.017 – 0.025	0.021	$(0.706 \pm 0.014^{+0.012}_{-0.034})$	2711	2.2
	450	0.025 – 0.037	0.032	$(0.582 \pm 0.011^{+0.007}_{-0.021})$	2962	1.1
	450	0.037 – 0.060	0.050	$(0.511 \pm 0.008^{+0.007}_{-0.005})$	3618	0.0
	450	0.060 – 0.100	0.080	$(0.425 \pm 0.007^{+0.007}_{-0.007})$	3305	0.0
	450	0.100 – 0.170	0.130	$(0.365 \pm 0.007^{+0.005}_{-0.002})$	3094	0.0
	450	0.170 – 0.300	0.250	$(0.257 \pm 0.005^{+0.007}_{-0.007})$	2612	0.0

Table 4: The reduced cross-section $\tilde{\sigma}$ for the reaction $e^+p \rightarrow e^+X$ ($\mathcal{L} = 135.5 \text{ pb}^{-1}$, corrected to $P_e = 0$). The bin range, bin centre (Q_c^2 and x_c) and measured cross section corrected to the electroweak Born level are shown. Other details as in Table 1. This table has two continuations.

Q^2 range (GeV ²)	Q_c^2 (GeV ²)	x range	x_c	$\bar{\sigma}$	N_{data}	$N_{\text{bg}}^{\text{MC}}$
530 – 710	650	0.010 – 0.017	0.013	$(0.865 \pm 0.014^{+0.024}_{-0.025})$	4045	29.0
	650	0.017 – 0.025	0.021	$(0.735 \pm 0.015^{+0.008}_{-0.018})$	2564	0.0
	650	0.025 – 0.037	0.032	$(0.609 \pm 0.013^{+0.009}_{-0.025})$	2043	1.1
	650	0.037 – 0.060	0.050	$(0.512 \pm 0.011^{+0.003}_{-0.010})$	2028	0.0
	650	0.060 – 0.100	0.080	$(0.434 \pm 0.010^{+0.002}_{-0.011})$	1809	0.0
	650	0.100 – 0.170	0.130	$(0.335 \pm 0.008^{+0.005}_{-0.003})$	1598	0.0
	650	0.170 – 0.300	0.250	$(0.238 \pm 0.006^{+0.003}_{-0.003})$	1453	0.0
710 – 900	800	0.009 – 0.017	0.013	$(0.836 \pm 0.017^{+0.027}_{-0.027})$	2600	41.2
	800	0.017 – 0.025	0.021	$(0.741 \pm 0.018^{+0.009}_{-0.014})$	1757	3.3
	800	0.025 – 0.037	0.032	$(0.610 \pm 0.015^{+0.007}_{-0.021})$	1747	7.9
	800	0.037 – 0.060	0.050	$(0.514 \pm 0.012^{+0.006}_{-0.022})$	1966	1.1
	800	0.060 – 0.100	0.080	$(0.454 \pm 0.011^{+0.003}_{-0.017})$	1768	0.0
	800	0.100 – 0.170	0.130	$(0.344 \pm 0.009^{+0.007}_{-0.011})$	1387	0.0
	800	0.170 – 0.300	0.250	$(0.243 \pm 0.007^{+0.006}_{-0.002})$	1110	0.0
900 – 1300	1200	0.010 – 0.017	0.014	$(0.815 \pm 0.021^{+0.073}_{-0.037})$	1631	36.5
	1200	0.017 – 0.025	0.021	$(0.737 \pm 0.017^{+0.018}_{-0.012})$	1819	12.2
	1200	0.025 – 0.037	0.032	$(0.626 \pm 0.014^{+0.007}_{-0.020})$	1863	0.0
	1200	0.037 – 0.060	0.050	$(0.513 \pm 0.011^{+0.008}_{-0.021})$	2209	0.0
	1200	0.060 – 0.100	0.080	$(0.423 \pm 0.009^{+0.005}_{-0.013})$	2037	1.1
	1200	0.100 – 0.170	0.130	$(0.352 \pm 0.008^{+0.003}_{-0.011})$	1845	0.0
	1200	0.170 – 0.300	0.250	$(0.247 \pm 0.006^{+0.002}_{-0.009})$	1459	0.0
1300 – 1800	1200	0.300 – 0.530	0.400	$(0.129 \pm 0.005^{+0.001}_{-0.003})$	624	0.0
	1500	0.017 – 0.025	0.021	$(0.724 \pm 0.024^{+0.086}_{-0.014})$	924	17.5
	1500	0.025 – 0.037	0.032	$(0.583 \pm 0.019^{+0.026}_{-0.008})$	952	1.5
	1500	0.037 – 0.060	0.050	$(0.532 \pm 0.015^{+0.005}_{-0.012})$	1309	1.1
	1500	0.060 – 0.100	0.080	$(0.446 \pm 0.012^{+0.004}_{-0.012})$	1303	0.0
	1500	0.100 – 0.150	0.130	$(0.373 \pm 0.012^{+0.003}_{-0.009})$	902	0.3
	1500	0.150 – 0.230	0.180	$(0.306 \pm 0.011^{+0.003}_{-0.006})$	789	0.0
1800 – 2500	1500	0.230 – 0.350	0.250	$(0.242 \pm 0.011^{+0.004}_{-0.003})$	528	0.0
	1500	0.350 – 0.530	0.400	$(0.119 \pm 0.007^{+0.002}_{-0.004})$	251	0.0
	2000	0.023 – 0.037	0.032	$(0.594 \pm 0.023^{+0.067}_{-0.012})$	701	12.2
	2000	0.037 – 0.060	0.050	$(0.495 \pm 0.018^{+0.011}_{-0.006})$	790	1.9
	2000	0.060 – 0.100	0.080	$(0.474 \pm 0.015^{+0.004}_{-0.019})$	940	1.1
	2000	0.100 – 0.150	0.130	$(0.352 \pm 0.014^{+0.005}_{-0.009})$	607	1.1
	2000	0.150 – 0.230	0.180	$(0.273 \pm 0.012^{+0.003}_{-0.007})$	499	0.0
	2000	0.230 – 0.350	0.250	$(0.247 \pm 0.013^{+0.004}_{-0.009})$	387	0.0
	2000	0.350 – 0.530	0.400	$(0.119 \pm 0.009^{+0.003}_{-0.001})$	180	0.0

Table 4: *Continuation 1.*

Q^2 range (GeV ²)	Q_c^2 (GeV ²)	x range	x_c	$\tilde{\sigma}$	N_{data}	$N_{\text{bg}}^{\text{MC}}$
2500 – 3500	3000	0.037 – 0.060	0.050	$(0.500 \pm 0.022^{+0.012}_{-0.012})$	502	2.2
	3000	0.060 – 0.100	0.080	$(0.429 \pm 0.018^{+0.004}_{-0.010})$	575	0.0
	3000	0.100 – 0.150	0.130	$(0.366 \pm 0.017^{+0.003}_{-0.014})$	448	0.0
	3000	0.150 – 0.230	0.180	$(0.276 \pm 0.015^{+0.004}_{-0.005})$	356	0.0
	3000	0.230 – 0.350	0.250	$(0.243 \pm 0.014^{+0.002}_{-0.008})$	286	0.0
	3000	0.350 – 0.530	0.400	$(0.121 \pm 0.011^{+0.004}_{-0.003})$	127	0.0
	3000	0.530 – 0.750	0.650	$(0.015^{+0.004}_{-0.003} \text{ } ^{+0.001}_{-0.000})$	21	0.0
3500 – 5600	5000	0.040 – 0.100	0.080	$(0.405 \pm 0.016^{+0.017}_{-0.007})$	628	3.9
	5000	0.100 – 0.150	0.130	$(0.328 \pm 0.018^{+0.003}_{-0.013})$	344	0.0
	5000	0.150 – 0.230	0.180	$(0.286 \pm 0.016^{+0.002}_{-0.007})$	333	0.0
	5000	0.230 – 0.350	0.250	$(0.215 \pm 0.014^{+0.002}_{-0.005})$	232	0.0
5600 – 9000	5000	0.350 – 0.530	0.400	$(0.135 \pm 0.012^{+0.002}_{-0.002})$	137	0.0
	8000	0.070 – 0.150	0.130	$(0.312 \pm 0.019^{+0.010}_{-0.012})$	277	0.0
	8000	0.150 – 0.230	0.180	$(0.239 \pm 0.019^{+0.002}_{-0.010})$	161	0.0
	8000	0.230 – 0.350	0.250	$(0.213 \pm 0.018^{+0.004}_{-0.007})$	136	0.0
	8000	0.350 – 0.530	0.400	$(0.104 \pm 0.013^{+0.003}_{-0.003})$	66	0.0
9000 – 15000	8000	0.530 – 0.750	0.650	$(0.017^{+0.006}_{-0.004} \text{ } ^{+0.002}_{-0.001})$	15	0.0
	12000	0.090 – 0.230	0.180	$(0.192 \pm 0.020^{+0.004}_{-0.006})$	95	0.0
	12000	0.230 – 0.350	0.250	$(0.152 \pm 0.020^{+0.002}_{-0.007})$	56	0.0
	12000	0.350 – 0.530	0.400	$(0.115 \pm 0.017^{+0.004}_{-0.005})$	44	0.0
15000 – 25000	20000	0.150 – 0.350	0.250	$(0.154^{+0.029}_{-0.025} \text{ } ^{+0.012}_{-0.010})$	38	0.0
	20000	0.350 – 0.750	0.400	$(0.064^{+0.021}_{-0.016} \text{ } ^{+0.005}_{-0.012})$	15	0.0
25000 – 50000	30000	0.250 – 0.750	0.400	$(0.040^{+0.024}_{-0.016} \text{ } ^{+0.001}_{-0.004})$	6	0.0

Table 4: *Continuation 2.*

Q^2 range (GeV ²)	Q_c^2 (GeV ²)	x range	x_c	$x\tilde{F}_3 \times 10$
1300 – 1800	1500	0.017 – 0.025	0.021	$0.24 \pm 0.20^{+0.52}_{-0.14}$
	1500	0.025 – 0.037	0.032	$0.39 \pm 0.23^{+0.24}_{-0.08}$
	1500	0.037 – 0.06	0.050	$-0.15 \pm 0.29^{+0.11}_{-0.18}$
	1500	0.06 – 0.1	0.080	$0.76 \pm 0.41^{+0.17}_{-0.33}$
	1500	0.1 – 0.15	0.130	$0.14 \pm 0.69^{+0.35}_{-0.46}$
	1500	0.15 – 0.23	0.180	$0.36 \pm 0.86^{+0.40}_{-0.46}$
	1500	0.23 – 0.35	0.250	$1.81 \pm 1.19^{+0.51}_{-0.49}$
	1500	0.35 – 0.53	0.400	$1.23 \pm 1.36^{+1.49}_{-0.96}$
1800 – 2500	2000	0.023 – 0.037	0.032	$0.29 \pm 0.21^{+0.46}_{-0.10}$
	2000	0.037 – 0.06	0.050	$0.82 \pm 0.26^{+0.13}_{-0.08}$
	2000	0.06 – 0.1	0.080	$-0.27 \pm 0.37^{+0.18}_{-0.38}$
	2000	0.1 – 0.15	0.130	$0.68 \pm 0.59^{+0.18}_{-0.30}$
	2000	0.15 – 0.23	0.180	$1.57 \pm 0.74^{+0.14}_{-0.40}$
	2000	0.23 – 0.35	0.250	$0.02 \pm 1.02^{+0.33}_{-0.62}$
	2000	0.35 – 0.53	0.400	$0.07 \pm 1.18^{+0.49}_{-0.50}$
2500 – 3500	3000	0.037 – 0.06	0.050	$0.57 \pm 0.21^{+0.12}_{-0.09}$
	3000	0.06 – 0.1	0.080	$0.90 \pm 0.29^{+0.09}_{-0.13}$
	3000	0.1 – 0.15	0.130	$0.24 \pm 0.45^{+0.10}_{-0.29}$
	3000	0.15 – 0.23	0.180	$1.23 \pm 0.57^{+0.17}_{-0.18}$
	3000	0.23 – 0.35	0.250	$1.71 \pm 0.80^{+0.84}_{-0.89}$
	3000	0.35 – 0.53	0.400	$0.90 \pm 0.96^{+0.40}_{-0.37}$
	3000	0.53 – 0.75	0.650	$0.24 \pm 0.41^{+0.26}_{-0.22}$
3500 – 5600	5000	0.04 – 0.1	0.080	$0.82 \pm 0.16^{+0.13}_{-0.05}$
	5000	0.1 – 0.15	0.130	$1.52 \pm 0.29^{+0.07}_{-0.15}$
	5000	0.15 – 0.23	0.180	$0.87 \pm 0.35^{+0.06}_{-0.12}$
	5000	0.23 – 0.35	0.250	$0.65 \pm 0.46^{+0.10}_{-0.14}$
	5000	0.35 – 0.53	0.400	$0.19 \pm 0.61^{+0.35}_{-0.36}$
5600 – 9000	8000	0.07 – 0.15	0.130	$1.70 \pm 0.21^{+0.08}_{-0.11}$
	8000	0.15 – 0.23	0.180	$1.87 \pm 0.28^{+0.11}_{-0.15}$
	8000	0.23 – 0.35	0.250	$1.33 \pm 0.37^{+0.17}_{-0.19}$
	8000	0.35 – 0.53	0.400	$0.24 \pm 0.42^{+0.20}_{-0.20}$
	8000	0.53 – 0.75	0.650	$0.06 \pm 0.22^{+0.08}_{-0.07}$
9000 – 15000	12000	0.09 – 0.23	0.180	$1.72 \pm 0.22^{+0.04}_{-0.12}$
	12000	0.23 – 0.35	0.250	$1.77 \pm 0.31^{+0.09}_{-0.09}$
	12000	0.35 – 0.53	0.400	$0.62 \pm 0.39^{+0.12}_{-0.12}$
15000 – 25000	20000	0.15 – 0.35	0.250	$1.68 \pm 0.27^{+0.17}_{-0.11}$
	20000	0.35 – 0.75	0.400	$1.01 \pm 0.27^{+0.09}_{-0.12}$
25000 – 50000	30000	0.25 – 0.75	0.400	$1.13 \pm 0.24^{+0.09}_{-0.09}$

Table 5: The structure-function $x\tilde{F}_3$ extracted using the e^+p data set ($\mathcal{L} = 135.5 \text{ pb}^{-1}$, corrected to $P_e = 0$) and previously published NC e^-p DIS results ($\mathcal{L} = 169.9 \text{ pb}^{-1}$, corrected to $P_e = 0$). The bin range and bin centre for Q^2 and x , and measured $x\tilde{F}_3$ are shown. Other details as in Table 1.

Q^2 (GeV ²)	x_c	$xF_3^{\gamma Z} \times 10$
1500	0.021	$2.85 \pm 1.21^{+1.57}_{-0.88}$
	0.032	$1.74 \pm 1.05^{+1.32}_{-0.62}$
	0.050	$3.35 \pm 0.84^{+0.46}_{-0.43}$
	0.080	$3.23 \pm 0.52^{+0.37}_{-0.21}$
	0.130	$4.91 \pm 0.50^{+0.17}_{-0.26}$
	0.180	$4.47 \pm 0.41^{+0.11}_{-0.22}$
	0.250	$3.86 \pm 0.41^{+0.20}_{-0.16}$
	0.400	$2.16 \pm 0.35^{+0.12}_{-0.14}$
	0.650	$0.32 \pm 0.73^{+0.28}_{-0.24}$

Table 6: *The interference structure-function $xF_3^{\gamma Z}$ evaluated at $Q^2 = 1\,500\text{ GeV}^2$ for x bins centred on x_c . The first (second) error on the measurement refers to the statistical (systematic) uncertainties.*

Q^2 range (GeV ²)	Q_c^2 (GeV ²)	x range	x_c	$\tilde{\sigma}$	N_{data}	$N_{\text{bg}}^{\text{MC}}$
185 – 240	200	0.004 – 0.006	0.005	$(1.126 \pm 0.013_{-0.018}^{+0.029})$	7884	61.0
	200	0.006 – 0.010	0.008	$(0.944 \pm 0.010_{-0.020}^{+0.008})$	9129	22.3
	200	0.010 – 0.017	0.013	$(0.797 \pm 0.008_{-0.022}^{+0.003})$	9345	8.1
	200	0.017 – 0.025	0.021	$(0.682 \pm 0.008_{-0.005}^{+0.013})$	6504	3.0
	200	0.025 – 0.037	0.032	$(0.563 \pm 0.007_{-0.001}^{+0.015})$	5678	0.0
	200	0.037 – 0.060	0.050	$(0.512 \pm 0.007_{-0.003}^{+0.011})$	6074	0.7
	200	0.060 – 0.120	0.080	$(0.434 \pm 0.005_{-0.001}^{+0.016})$	8126	0.0
240 – 310	200	0.120 – 0.250	0.180	$(0.346 \pm 0.005_{-0.008}^{+0.006})$	5163	0.0
	250	0.006 – 0.010	0.008	$(0.939 \pm 0.013_{-0.010}^{+0.020})$	5432	20.1
	250	0.010 – 0.017	0.013	$(0.822 \pm 0.010_{-0.035}^{+0.007})$	6209	6.3
	250	0.017 – 0.025	0.021	$(0.711 \pm 0.010_{-0.011}^{+0.003})$	4663	2.6
	250	0.025 – 0.037	0.032	$(0.606 \pm 0.009_{-0.012}^{+0.012})$	4518	0.7
	250	0.037 – 0.060	0.050	$(0.514 \pm 0.008_{-0.008}^{+0.013})$	4529	0.0
	250	0.060 – 0.120	0.080	$(0.437 \pm 0.006_{-0.005}^{+0.010})$	5960	0.0
310 – 410	250	0.120 – 0.250	0.180	$(0.340 \pm 0.005_{-0.009}^{+0.006})$	4741	0.0
	350	0.006 – 0.010	0.008	$(0.963 \pm 0.017_{-0.007}^{+0.030})$	3313	15.5
	350	0.010 – 0.017	0.013	$(0.817 \pm 0.013_{-0.019}^{+0.011})$	4131	3.3
	350	0.017 – 0.025	0.021	$(0.689 \pm 0.012_{-0.010}^{+0.010})$	3088	0.7
	350	0.025 – 0.037	0.032	$(0.576 \pm 0.011_{-0.003}^{+0.019})$	2847	0.7
	350	0.037 – 0.060	0.050	$(0.520 \pm 0.009_{-0.007}^{+0.011})$	3181	0.7
	350	0.060 – 0.120	0.080	$(0.426 \pm 0.007_{-0.005}^{+0.016})$	4063	0.0
410 – 530	350	0.120 – 0.250	0.180	$(0.336 \pm 0.005_{-0.005}^{+0.008})$	3834	0.0
	450	0.006 – 0.010	0.008	$(1.044 \pm 0.020_{-0.018}^{+0.020})$	2718	26.0
	450	0.010 – 0.017	0.013	$(0.828 \pm 0.019_{-0.018}^{+0.013})$	1957	3.8
	450	0.017 – 0.025	0.021	$(0.715 \pm 0.018_{-0.034}^{+0.014})$	1607	1.3
	450	0.025 – 0.037	0.032	$(0.598 \pm 0.014_{-0.022}^{+0.008})$	1779	0.6
	450	0.037 – 0.060	0.050	$(0.504 \pm 0.011_{-0.006}^{+0.005})$	2087	0.0
	450	0.060 – 0.100	0.080	$(0.434 \pm 0.010_{-0.008}^{+0.009})$	1968	0.0
	450	0.100 – 0.170	0.130	$(0.382 \pm 0.009_{-0.002}^{+0.005})$	1891	0.0
	450	0.170 – 0.300	0.250	$(0.264 \pm 0.007_{-0.008}^{+0.006})$	1571	0.0

Table 7: The reduced cross-section $\tilde{\sigma}$ for the reaction $e^+p \rightarrow e^+X$ ($\mathcal{L} = 78.8 \text{ pb}^{-1}$, $P_e = +0.32$). The bin range, bin centre (Q_c^2 and x_c) and measured cross section corrected to the electroweak Born level are shown. Other details as in Table 1. This table has two continuations.

Q^2 range (GeV ²)	Q_c^2 (GeV ²)	x range	x_c	$\bar{\sigma}$	N_{data}	$N_{\text{bg}}^{\text{MC}}$
530 – 710	650	0.010 – 0.017	0.013	$(0.899 \pm 0.018^{+0.019}_{-0.025})$	2458	17.2
	650	0.017 – 0.025	0.021	$(0.763 \pm 0.019^{+0.007}_{-0.018})$	1551	0.0
	650	0.025 – 0.037	0.032	$(0.627 \pm 0.018^{+0.009}_{-0.025})$	1222	0.7
	650	0.037 – 0.060	0.050	$(0.520 \pm 0.015^{+0.003}_{-0.010})$	1199	0.0
	650	0.060 – 0.100	0.080	$(0.440 \pm 0.013^{+0.004}_{-0.011})$	1071	0.0
	650	0.100 – 0.170	0.130	$(0.320 \pm 0.011^{+0.006}_{-0.003})$	892	0.0
710 – 900	650	0.170 – 0.300	0.250	$(0.244 \pm 0.008^{+0.004}_{-0.004})$	869	0.0
	800	0.009 – 0.017	0.013	$(0.873 \pm 0.022^{+0.022}_{-0.027})$	1590	25.2
	800	0.017 – 0.025	0.021	$(0.748 \pm 0.023^{+0.008}_{-0.012})$	1039	1.9
	800	0.025 – 0.037	0.032	$(0.605 \pm 0.019^{+0.006}_{-0.020})$	1014	4.6
	800	0.037 – 0.060	0.050	$(0.534 \pm 0.015^{+0.004}_{-0.023})$	1192	0.7
	800	0.060 – 0.100	0.080	$(0.455 \pm 0.014^{+0.003}_{-0.017})$	1031	0.0
900 – 1300	800	0.100 – 0.170	0.130	$(0.363 \pm 0.012^{+0.008}_{-0.012})$	850	0.0
	800	0.170 – 0.300	0.250	$(0.243 \pm 0.010^{+0.006}_{-0.003})$	646	0.0
	1200	0.010 – 0.017	0.014	$(0.853 \pm 0.028^{+0.065}_{-0.038})$	994	21.5
	1200	0.017 – 0.025	0.021	$(0.758 \pm 0.023^{+0.017}_{-0.010})$	1090	7.1
	1200	0.025 – 0.037	0.032	$(0.641 \pm 0.019^{+0.006}_{-0.020})$	1114	0.0
	1200	0.037 – 0.060	0.050	$(0.531 \pm 0.015^{+0.009}_{-0.022})$	1334	0.0
1300 – 1800	1200	0.060 – 0.100	0.080	$(0.437 \pm 0.012^{+0.005}_{-0.013})$	1227	0.7
	1200	0.100 – 0.170	0.130	$(0.365 \pm 0.011^{+0.004}_{-0.012})$	1115	0.0
	1200	0.170 – 0.300	0.250	$(0.259 \pm 0.009^{+0.002}_{-0.010})$	893	0.0
	1200	0.300 – 0.530	0.400	$(0.133 \pm 0.007^{+0.002}_{-0.003})$	375	0.0
	1500	0.017 – 0.025	0.021	$(0.747 \pm 0.032^{+0.088}_{-0.013})$	556	10.5
	1500	0.025 – 0.037	0.032	$(0.585 \pm 0.025^{+0.040}_{-0.007})$	558	0.6
1800 – 2500	1500	0.037 – 0.060	0.050	$(0.562 \pm 0.020^{+0.005}_{-0.013})$	806	0.6
	1500	0.060 – 0.100	0.080	$(0.458 \pm 0.016^{+0.006}_{-0.012})$	780	0.0
	1500	0.100 – 0.150	0.130	$(0.387 \pm 0.017^{+0.003}_{-0.010})$	547	0.0
	1500	0.150 – 0.230	0.180	$(0.329 \pm 0.015^{+0.003}_{-0.007})$	496	0.0
	1500	0.230 – 0.350	0.250	$(0.249 \pm 0.014^{+0.004}_{-0.003})$	318	0.0
	1500	0.350 – 0.530	0.400	$(0.115 \pm 0.010^{+0.002}_{-0.004})$	142	0.0
1800 – 2500	2000	0.023 – 0.037	0.032	$(0.584 \pm 0.030^{+0.082}_{-0.011})$	402	7.1
	2000	0.037 – 0.060	0.050	$(0.522 \pm 0.024^{+0.006}_{-0.008})$	486	1.3
	2000	0.060 – 0.100	0.080	$(0.503 \pm 0.021^{+0.004}_{-0.020})$	582	0.7
	2000	0.100 – 0.150	0.130	$(0.355 \pm 0.019^{+0.003}_{-0.009})$	358	0.7
	2000	0.150 – 0.230	0.180	$(0.275 \pm 0.016^{+0.001}_{-0.008})$	294	0.0
	2000	0.230 – 0.350	0.250	$(0.254 \pm 0.017^{+0.004}_{-0.010})$	233	0.0
	2000	0.350 – 0.530	0.400	$(0.120 \pm 0.012^{+0.007}_{-0.001})$	106	0.0

Table 7: *Continuation 1.*

Q^2 range (GeV ²)	Q_c^2 (GeV ²)	x range	x_c	$\tilde{\sigma}$	N_{data}	$N_{\text{bg}}^{\text{MC}}$
2500 – 3500	3000	0.037 – 0.060	0.050	$(0.497 \pm 0.029^{+0.013}_{-0.012})$	290	1.3
	3000	0.060 – 0.100	0.080	$(0.434 \pm 0.024^{+0.009}_{-0.009})$	338	0.0
	3000	0.100 – 0.150	0.130	$(0.380 \pm 0.023^{+0.003}_{-0.015})$	271	0.0
	3000	0.150 – 0.230	0.180	$(0.300 \pm 0.020^{+0.005}_{-0.004})$	225	0.0
	3000	0.230 – 0.350	0.250	$(0.264 \pm 0.020^{+0.002}_{-0.008})$	181	0.0
	3000	0.350 – 0.530	0.400	$(0.114 \pm 0.014^{+0.003}_{-0.003})$	70	0.0
	3000	0.530 – 0.750	0.650	$(0.016^{+0.006}_{-0.004} \text{ } ^{+0.002}_{-0.000})$	13	0.0
3500 – 5600	5000	0.040 – 0.100	0.080	$(0.450 \pm 0.023^{+0.017}_{-0.006})$	401	2.3
	5000	0.100 – 0.150	0.130	$(0.370 \pm 0.025^{+0.007}_{-0.015})$	224	0.0
	5000	0.150 – 0.230	0.180	$(0.326 \pm 0.022^{+0.002}_{-0.008})$	220	0.0
	5000	0.230 – 0.350	0.250	$(0.235 \pm 0.019^{+0.002}_{-0.007})$	147	0.0
5600 – 9000	5000	0.350 – 0.530	0.400	$(0.149 \pm 0.016^{+0.003}_{-0.003})$	88	0.0
	8000	0.070 – 0.150	0.130	$(0.339 \pm 0.026^{+0.010}_{-0.018})$	173	0.0
	8000	0.150 – 0.230	0.180	$(0.229 \pm 0.024^{+0.003}_{-0.009})$	89	0.0
	8000	0.230 – 0.350	0.250	$(0.241 \pm 0.026^{+0.004}_{-0.009})$	89	0.0
	8000	0.350 – 0.530	0.400	$(0.111^{+0.020}_{-0.017} \text{ } ^{+0.006}_{-0.003})$	41	0.0
9000 – 15000	8000	0.530 – 0.750	0.650	$(0.020^{+0.008}_{-0.006} \text{ } ^{+0.002}_{-0.002})$	10	0.0
	12000	0.090 – 0.230	0.180	$(0.218 \pm 0.028^{+0.007}_{-0.013})$	62	0.0
	12000	0.230 – 0.350	0.250	$(0.188^{+0.035}_{-0.030} \text{ } ^{+0.004}_{-0.013})$	40	0.0
	12000	0.350 – 0.530	0.400	$(0.148^{+0.030}_{-0.026} \text{ } ^{+0.003}_{-0.008})$	33	0.0
15000 – 25000	20000	0.150 – 0.350	0.250	$(0.135^{+0.039}_{-0.031} \text{ } ^{+0.020}_{-0.008})$	19	0.0
	20000	0.350 – 0.750	0.400	$(0.059^{+0.029}_{-0.020} \text{ } ^{+0.006}_{-0.008})$	8	0.0
25000 – 50000	30000	0.250 – 0.750	0.400	$(0.023^{+0.031}_{-0.015} \text{ } ^{+0.001}_{-0.022})$	2	0.0

Table 7: *Continuation 2.*

Q^2 range (GeV ²)	Q_c^2 (GeV ²)	x range	x_c	$\tilde{\sigma}$	N_{data}	$N_{\text{bg}}^{\text{MC}}$
185 – 240	200	0.004 – 0.006	0.005	$(1.089 \pm 0.015^{+0.029}_{-0.015})$	5429	47.1
	200	0.006 – 0.010	0.008	$(0.947 \pm 0.012^{+0.010}_{-0.026})$	6518	16.5
	200	0.010 – 0.017	0.013	$(0.807 \pm 0.010^{+0.003}_{-0.022})$	6729	6.0
	200	0.017 – 0.025	0.021	$(0.679 \pm 0.010^{+0.013}_{-0.005})$	4603	2.1
	200	0.025 – 0.037	0.032	$(0.571 \pm 0.009^{+0.016}_{-0.003})$	4089	0.0
	200	0.037 – 0.060	0.050	$(0.510 \pm 0.008^{+0.011}_{-0.002})$	4301	0.5
	200	0.060 – 0.120	0.080	$(0.431 \pm 0.006^{+0.015}_{-0.001})$	5741	0.0
240 – 310	200	0.120 – 0.250	0.180	$(0.346 \pm 0.006^{+0.006}_{-0.009})$	3660	0.0
	250	0.006 – 0.010	0.008	$(0.916 \pm 0.015^{+0.026}_{-0.012})$	3758	14.8
	250	0.010 – 0.017	0.013	$(0.821 \pm 0.012^{+0.005}_{-0.034})$	4402	3.7
	250	0.017 – 0.025	0.021	$(0.667 \pm 0.012^{+0.009}_{-0.004})$	3107	3.7
	250	0.025 – 0.037	0.032	$(0.557 \pm 0.010^{+0.011}_{-0.009})$	2948	0.5
	250	0.037 – 0.060	0.050	$(0.513 \pm 0.009^{+0.012}_{-0.009})$	3211	0.0
310 – 410	250	0.060 – 0.120	0.080	$(0.432 \pm 0.007^{+0.010}_{-0.004})$	4182	0.0
	250	0.120 – 0.250	0.180	$(0.334 \pm 0.006^{+0.004}_{-0.007})$	3301	0.0
	350	0.006 – 0.010	0.008	$(0.929 \pm 0.020^{+0.038}_{-0.009})$	2266	11.8
	350	0.010 – 0.017	0.013	$(0.800 \pm 0.015^{+0.009}_{-0.018})$	2869	2.8
	350	0.017 – 0.025	0.021	$(0.652 \pm 0.014^{+0.009}_{-0.010})$	2079	0.2
	350	0.025 – 0.037	0.032	$(0.576 \pm 0.013^{+0.016}_{-0.006})$	2022	0.4
410 – 530	350	0.037 – 0.060	0.050	$(0.489 \pm 0.011^{+0.011}_{-0.004})$	2125	0.5
	350	0.060 – 0.120	0.080	$(0.407 \pm 0.008^{+0.016}_{-0.003})$	2760	0.0
	350	0.120 – 0.250	0.180	$(0.310 \pm 0.006^{+0.006}_{-0.003})$	2506	0.0
	450	0.006 – 0.010	0.008	$(0.997 \pm 0.024^{+0.021}_{-0.023})$	1830	18.9
	450	0.010 – 0.017	0.013	$(0.802 \pm 0.022^{+0.010}_{-0.020})$	1347	2.9
	450	0.017 – 0.025	0.021	$(0.696 \pm 0.021^{+0.010}_{-0.034})$	1104	0.9
410 – 530	450	0.025 – 0.037	0.032	$(0.563 \pm 0.016^{+0.007}_{-0.020})$	1183	0.5
	450	0.037 – 0.060	0.050	$(0.523 \pm 0.013^{+0.010}_{-0.003})$	1531	0.0
	450	0.060 – 0.100	0.080	$(0.415 \pm 0.011^{+0.007}_{-0.008})$	1337	0.0
	450	0.100 – 0.170	0.130	$(0.342 \pm 0.010^{+0.007}_{-0.002})$	1203	0.0
	450	0.170 – 0.300	0.250	$(0.248 \pm 0.008^{+0.009}_{-0.007})$	1041	0.0

Table 8: The reduced cross-section $\tilde{\sigma}$ for the reaction $e^+p \rightarrow e^+X$ ($\mathcal{L} = 56.7 \text{ pb}^{-1}$, $P_e = -0.36$). The bin range, bin centre (Q_c^2 and x_c) and measured cross section corrected to the electroweak Born level are shown. Other details as in Table 1. This table has two continuations.

Q^2 range (GeV ²)	Q_c^2 (GeV ²)	x range	x_c	$\bar{\sigma}$	N_{data}	$N_{\text{bg}}^{\text{MC}}$
530 – 710	650	0.010 – 0.017	0.013	$(0.822 \pm 0.021^{+0.033}_{-0.026})$	1587	11.8
	650	0.017 – 0.025	0.021	$(0.699 \pm 0.022^{+0.010}_{-0.019})$	1013	0.0
	650	0.025 – 0.037	0.032	$(0.587 \pm 0.020^{+0.010}_{-0.024})$	821	0.5
	650	0.037 – 0.060	0.050	$(0.503 \pm 0.017^{+0.004}_{-0.011})$	829	0.0
	650	0.060 – 0.100	0.080	$(0.426 \pm 0.016^{+0.002}_{-0.012})$	738	0.0
	650	0.100 – 0.170	0.130	$(0.358 \pm 0.013^{+0.003}_{-0.003})$	706	0.0
	650	0.170 – 0.300	0.250	$(0.232 \pm 0.010^{+0.002}_{-0.003})$	584	0.0
710 – 900	800	0.009 – 0.017	0.013	$(0.788 \pm 0.025^{+0.034}_{-0.028})$	1010	16.0
	800	0.017 – 0.025	0.021	$(0.734 \pm 0.027^{+0.012}_{-0.017})$	718	1.4
	800	0.025 – 0.037	0.032	$(0.620 \pm 0.023^{+0.012}_{-0.022})$	733	3.3
	800	0.037 – 0.060	0.050	$(0.489 \pm 0.018^{+0.010}_{-0.022})$	774	0.4
	800	0.060 – 0.100	0.080	$(0.456 \pm 0.017^{+0.005}_{-0.017})$	737	0.0
	800	0.100 – 0.170	0.130	$(0.320 \pm 0.014^{+0.005}_{-0.010})$	537	0.0
	800	0.170 – 0.300	0.250	$(0.244 \pm 0.011^{+0.007}_{-0.003})$	464	0.0
900 – 1300	1200	0.010 – 0.017	0.014	$(0.769 \pm 0.031^{+0.085}_{-0.037})$	637	14.9
	1200	0.017 – 0.025	0.021	$(0.715 \pm 0.027^{+0.019}_{-0.015})$	729	5.1
	1200	0.025 – 0.037	0.032	$(0.608 \pm 0.022^{+0.011}_{-0.020})$	749	0.0
	1200	0.037 – 0.060	0.050	$(0.490 \pm 0.017^{+0.007}_{-0.021})$	875	0.0
	1200	0.060 – 0.100	0.080	$(0.406 \pm 0.014^{+0.006}_{-0.013})$	810	0.5
	1200	0.100 – 0.170	0.130	$(0.336 \pm 0.012^{+0.003}_{-0.011})$	730	0.0
	1200	0.170 – 0.300	0.250	$(0.232 \pm 0.010^{+0.002}_{-0.008})$	566	0.0
1300 – 1800	1200	0.300 – 0.530	0.400	$(0.125 \pm 0.008^{+0.002}_{-0.004})$	249	0.0
	1500	0.017 – 0.025	0.021	$(0.699 \pm 0.037^{+0.083}_{-0.020})$	368	7.1
	1500	0.025 – 0.037	0.032	$(0.585 \pm 0.030^{+0.011}_{-0.011})$	394	0.9
	1500	0.037 – 0.060	0.050	$(0.496 \pm 0.022^{+0.007}_{-0.011})$	503	0.5
	1500	0.060 – 0.100	0.080	$(0.434 \pm 0.019^{+0.005}_{-0.012})$	523	0.0
	1500	0.100 – 0.150	0.130	$(0.356 \pm 0.019^{+0.005}_{-0.009})$	355	0.3
	1500	0.150 – 0.230	0.180	$(0.276 \pm 0.016^{+0.004}_{-0.005})$	293	0.0
1800 – 2500	1500	0.230 – 0.350	0.250	$(0.234 \pm 0.016^{+0.005}_{-0.004})$	210	0.0
	1500	0.350 – 0.530	0.400	$(0.126 \pm 0.012^{+0.004}_{-0.004})$	109	0.0
	2000	0.023 – 0.037	0.032	$(0.615 \pm 0.036^{+0.048}_{-0.015})$	299	5.1
	2000	0.037 – 0.060	0.050	$(0.463 \pm 0.027^{+0.029}_{-0.007})$	304	0.6
	2000	0.060 – 0.100	0.080	$(0.439 \pm 0.023^{+0.006}_{-0.018})$	358	0.4
	2000	0.100 – 0.150	0.130	$(0.351 \pm 0.022^{+0.006}_{-0.009})$	249	0.4
	2000	0.150 – 0.230	0.180	$(0.273 \pm 0.019^{+0.006}_{-0.007})$	205	0.0
	2000	0.230 – 0.350	0.250	$(0.239 \pm 0.019^{+0.005}_{-0.009})$	154	0.0
	2000	0.350 – 0.530	0.400	$(0.120 \pm 0.014^{+0.002}_{-0.004})$	74	0.0

Table 8: *Continuation 1.*

Q^2 range (GeV ²)	Q_c^2 (GeV ²)	x range	x_c	$\tilde{\sigma}$	N_{data}	$N_{\text{bg}}^{\text{MC}}$
2500 – 3500	3000	0.037 – 0.060	0.050	$(0.511 \pm 0.035^{+0.012}_{-0.013})$	212	0.9
	3000	0.060 – 0.100	0.080	$(0.429 \pm 0.028^{+0.006}_{-0.015})$	237	0.0
	3000	0.100 – 0.150	0.130	$(0.350 \pm 0.026^{+0.005}_{-0.015})$	177	0.0
	3000	0.150 – 0.230	0.180	$(0.247 \pm 0.022^{+0.005}_{-0.008})$	131	0.0
	3000	0.230 – 0.350	0.250	$(0.217 \pm 0.021^{+0.003}_{-0.012})$	105	0.0
	3000	0.350 – 0.530	0.400	$(0.133 \pm 0.018^{+0.006}_{-0.004})$	57	0.0
3500 – 5600	3000	0.530 – 0.750	0.650	$(0.014^{+0.007}_{-0.005} \text{ } ^{+0.001}_{-0.000})$	8	0.0
	5000	0.040 – 0.100	0.080	$(0.351 \pm 0.023^{+0.016}_{-0.010})$	227	1.7
	5000	0.100 – 0.150	0.130	$(0.276 \pm 0.025^{+0.005}_{-0.014})$	120	0.0
	5000	0.150 – 0.230	0.180	$(0.235 \pm 0.022^{+0.003}_{-0.007})$	113	0.0
5600 – 9000	5000	0.230 – 0.350	0.250	$(0.191 \pm 0.021^{+0.004}_{-0.005})$	85	0.0
	5000	0.350 – 0.530	0.400	$(0.118 \pm 0.017^{+0.002}_{-0.003})$	49	0.0
	8000	0.070 – 0.150	0.130	$(0.281 \pm 0.028^{+0.012}_{-0.009})$	104	0.0
	8000	0.150 – 0.230	0.180	$(0.258 \pm 0.030^{+0.003}_{-0.016})$	72	0.0
	8000	0.230 – 0.350	0.250	$(0.179 \pm 0.026^{+0.006}_{-0.005})$	47	0.0
9000 – 15000	8000	0.350 – 0.530	0.400	$(0.096^{+0.023}_{-0.019} \text{ } ^{+0.002}_{-0.007})$	25	0.0
	8000	0.530 – 0.750	0.650	$(0.014^{+0.010}_{-0.006} \text{ } ^{+0.003}_{-0.003})$	5	0.0
	12000	0.090 – 0.230	0.180	$(0.161^{+0.033}_{-0.028} \text{ } ^{+0.012}_{-0.007})$	33	0.0
	12000	0.230 – 0.350	0.250	$(0.106^{+0.034}_{-0.026} \text{ } ^{+0.002}_{-0.003})$	16	0.0
	12000	0.350 – 0.530	0.400	$(0.070^{+0.028}_{-0.021} \text{ } ^{+0.008}_{-0.006})$	11	0.0
15000 – 25000	20000	0.150 – 0.350	0.250	$(0.185^{+0.053}_{-0.042} \text{ } ^{+0.017}_{-0.020})$	19	0.0
	20000	0.350 – 0.750	0.400	$(0.073^{+0.040}_{-0.027} \text{ } ^{+0.009}_{-0.026})$	7	0.0
25000 – 50000	30000	0.250 – 0.750	0.400	$(0.065^{+0.052}_{-0.031} \text{ } ^{+0.026}_{-0.003})$	4	0.0

Table 8: *Continuation 2.*

Q^2 range (GeV ²)	Q_c^2 (GeV ²)	$d\sigma/dQ^2$ (pb/GeV ²)	N_{data}	$N_{\text{bg}}^{\text{MC}}$
185.0 – 300.0	250	$(1.07 \pm 0.00^{+0.01}_{-0.01}) \times 10^1$	96158	149.8
300.0 – 400.0	350	$(4.74 \pm 0.03^{+0.07}_{-0.03})$	28667	33.6
400.0 – 475.7	440	$(2.73 \pm 0.03^{+0.05}_{-0.05})$	11858	36.2
475.7 – 565.7	520	$(1.83 \pm 0.02^{+0.03}_{-0.05})$	8698	22.7
565.7 – 672.7	620	$(1.19 \pm 0.02^{+0.02}_{-0.03})$	6108	22.4
672.7 – 800.0	730	$(8.02 \pm 0.11^{+0.10}_{-0.24}) \times 10^{-1}$	5859	20.0
800.0 – 1050.0	900	$(4.75 \pm 0.05^{+0.07}_{-0.17}) \times 10^{-1}$	7622	29.7
1050.0 – 1460.0	1230	$(2.11 \pm 0.03^{+0.05}_{-0.05}) \times 10^{-1}$	5875	32.9
1460.0 – 2080.0	1730	$(9.00 \pm 0.15^{+0.23}_{-0.13}) \times 10^{-2}$	3832	14.9
2080.0 – 3120.0	2500	$(3.28 \pm 0.07^{+0.07}_{-0.05}) \times 10^{-2}$	2298	6.1
3120.0 – 5220.0	3900	$(1.04 \pm 0.03^{+0.02}_{-0.02}) \times 10^{-2}$	1416	2.9
5220.0 – 12500.0	7000	$(1.73 \pm 0.07^{+0.02}_{-0.05}) \times 10^{-3}$	616	0.0
12500.0 – 51200.0	22400	$(2.03 \pm 0.26^{+0.02}_{-0.05}) \times 10^{-5}$	60	0.0

Table 9: The single-differential cross-section $d\sigma/dQ^2$ ($y < 0.9$, $y(1-x)^2 > 0.004$) for the reaction $e^+p \rightarrow e^+X$ ($\mathcal{L} = 78.8 \text{ pb}^{-1}$, $P_e = +0.32$). The bin range, bin centre (Q_c^2) and measured cross section corrected to the electroweak Born level are shown. Other details as in Table 1.

$Q^2 >$ (GeV ²)	x range	x_c	$d\sigma/dx$ (pb)	N_{data}	$N_{\text{bg}}^{\text{MC}}$
185	$(0.63 - 1.00) \times 10^{-2}$	0.794×10^{-2}	$(8.80 \pm 0.06^{+0.12}_{-0.13}) \times 10^4$	20397	91.9
	$(0.10 - 0.16) \times 10^{-1}$	0.126×10^{-1}	$(5.88 \pm 0.04^{+0.06}_{-0.17}) \times 10^4$	23452	71.7
	$(0.16 - 0.25) \times 10^{-1}$	0.200×10^{-1}	$(3.69 \pm 0.02^{+0.03}_{-0.03}) \times 10^4$	23332	49.5
	$(0.25 - 0.40) \times 10^{-1}$	0.316×10^{-1}	$(2.12 \pm 0.01^{+0.02}_{-0.01}) \times 10^4$	22669	17.5
	$(0.40 - 0.63) \times 10^{-1}$	0.501×10^{-1}	$(1.25 \pm 0.01^{+0.01}_{-0.01}) \times 10^4$	19901	3.3
	$(0.63 - 1.00) \times 10^{-1}$	0.794×10^{-1}	$(6.98 \pm 0.05^{+0.08}_{-0.03}) \times 10^3$	18738	2.9
	0.10 – 0.16	0.126	$(3.97 \pm 0.03^{+0.05}_{-0.02}) \times 10^3$	18025	0.7
	0.16 – 0.25	0.200	$(2.09 \pm 0.02^{+0.04}_{-0.05}) \times 10^3$	11263	0.0
3000	$(0.40 - 0.63) \times 10^{-1}$	0.501×10^{-1}	$(1.81 \pm 0.11^{+0.08}_{-0.03}) \times 10^2$	269	0.6
	$(0.63 - 1.00) \times 10^{-1}$	0.794×10^{-1}	$(1.69 \pm 0.08^{+0.04}_{-0.02}) \times 10^2$	437	2.3
	0.10 – 0.16	0.126	$(1.28 \pm 0.06^{+0.01}_{-0.05}) \times 10^2$	542	0.0
	0.16 – 0.25	0.200	$(7.46 \pm 0.34^{+0.06}_{-0.19}) \times 10^1$	471	0.0
	0.25 – 0.40	0.316	$(3.41 \pm 0.18^{+0.08}_{-0.09}) \times 10^1$	350	0.0
	0.40 – 0.75	0.687	$(1.29 \pm 0.11^{+0.03}_{-0.02})$	151	0.0

Table 10: The single-differential cross-section $d\sigma/dx$ ($y < 0.9$, $y(1-x)^2 > 0.004$) for $Q^2 > 185 \text{ GeV}^2$ and $Q^2 > 3000 \text{ GeV}^2$ for the reaction $e^+p \rightarrow e^+X$ ($\mathcal{L} = 78.8 \text{ pb}^{-1}$, $P_e = +0.32$). The Q^2 and bin range, bin centre (x_c) and measured cross section corrected to the electroweak Born level are shown. Other details as in Table 1.

$Q^2 >$ (GeV ²)	y range	y_c	$d\sigma/dy$ (pb)	N_{data}	$N_{\text{bg}}^{\text{MC}}$
185	0.00 – 0.05	0.025	$(1.65 \pm 0.01_{-0.01}^{+0.02}) \times 10^4$	44541	0.0
	0.05 – 0.10	0.075	$(8.19 \pm 0.05_{-0.05}^{+0.10}) \times 10^3$	29853	4.4
	0.10 – 0.15	0.125	$(5.73 \pm 0.04_{-0.05}^{+0.03}) \times 10^3$	20723	5.3
	0.15 – 0.20	0.175	$(4.40 \pm 0.04_{-0.14}^{+0.02}) \times 10^3$	15423	15.0
	0.20 – 0.25	0.225	$(3.66 \pm 0.03_{-0.21}^{+0.03}) \times 10^3$	12419	11.7
	0.25 – 0.30	0.275	$(2.96 \pm 0.03_{-0.03}^{+0.03}) \times 10^3$	9588	10.2
	0.30 – 0.35	0.325	$(2.58 \pm 0.03_{-0.03}^{+0.04}) \times 10^3$	8283	25.2
	0.35 – 0.40	0.375	$(2.26 \pm 0.03_{-0.03}^{+0.03}) \times 10^3$	7167	24.7
	0.40 – 0.45	0.425	$(2.01 \pm 0.03_{-0.02}^{+0.03}) \times 10^3$	6164	35.7
	0.45 – 0.50	0.475	$(1.76 \pm 0.02_{-0.02}^{+0.05}) \times 10^3$	5223	28.7
	0.50 – 0.55	0.525	$(1.56 \pm 0.02_{-0.01}^{+0.04}) \times 10^3$	4534	32.9
	0.55 – 0.60	0.575	$(1.46 \pm 0.02_{-0.03}^{+0.04}) \times 10^3$	4079	38.4
	0.60 – 0.65	0.625	$(1.31 \pm 0.02_{-0.04}^{+0.03}) \times 10^3$	3415	37.2
	0.65 – 0.70	0.675	$(1.22 \pm 0.02_{-0.05}^{+0.05}) \times 10^3$	2788	25.1
	0.70 – 0.75	0.725	$(1.13 \pm 0.02_{-0.05}^{+0.07}) \times 10^3$	2097	28.8
	0.75 – 0.90	0.825	$(9.76 \pm 0.19_{-0.46}^{+0.69}) \times 10^2$	2685	58.5
3000	0.05 – 0.10	0.075	$(3.50 \pm 0.34_{-0.03}^{+0.05}) \times 10^1$	109	0.0
	0.10 – 0.15	0.125	$(5.86 \pm 0.41_{-0.14}^{+0.08}) \times 10^1$	201	0.0
	0.15 – 0.20	0.175	$(6.38 \pm 0.43_{-0.13}^{+0.04}) \times 10^1$	225	0.0
	0.20 – 0.25	0.225	$(6.32 \pm 0.42_{-0.22}^{+0.08}) \times 10^1$	226	0.0
	0.25 – 0.30	0.275	$(5.59 \pm 0.39_{-0.21}^{+0.03}) \times 10^1$	204	0.0
	0.30 – 0.35	0.325	$(5.66 \pm 0.40_{-0.14}^{+0.05}) \times 10^1$	206	0.0
	0.35 – 0.40	0.375	$(3.90 \pm 0.33_{-0.20}^{+0.07}) \times 10^1$	142	0.0
	0.40 – 0.45	0.425	$(3.56 \pm 0.31_{-0.10}^{+0.05}) \times 10^1$	130	0.0
	0.45 – 0.50	0.475	$(3.62 \pm 0.32_{-0.10}^{+0.14}) \times 10^1$	131	0.0
	0.50 – 0.55	0.525	$(2.89 \pm 0.29_{-0.14}^{+0.03}) \times 10^1$	103	0.0
	0.55 – 0.60	0.575	$(3.19 \pm 0.30_{-0.04}^{+0.23}) \times 10^1$	112	0.0
	0.60 – 0.65	0.625	$(2.55 \pm 0.26_{-0.04}^{+0.13}) \times 10^1$	93	2.3
	0.65 – 0.70	0.675	$(2.69 \pm 0.28_{-0.15}^{+0.05}) \times 10^1$	92	0.0
	0.70 – 0.75	0.725	$(2.39 \pm 0.27_{-0.18}^{+0.07}) \times 10^1$	79	0.0
	0.75 – 0.80	0.775	$(2.17 \pm 0.26_{-0.11}^{+0.10}) \times 10^1$	71	0.0
	0.80 – 0.85	0.825	$(2.16 \pm 0.26_{-0.07}^{+0.28}) \times 10^1$	68	0.6
0.85 – 0.90	0.875	$(1.98 \pm 0.28_{-0.20}^{+0.22}) \times 10^1$	52	0.0	

Table 11: The single-differential cross-section $d\sigma/dy$ for $Q^2 > 185 \text{ GeV}^2$ and $Q^2 > 3000 \text{ GeV}^2$ ($y(1-x)^2 > 0.004$) for the reaction $e^+p \rightarrow e^+X$ ($\mathcal{L} = 78.8 \text{ pb}^{-1}$, $P_e = +0.32$). The Q^2 and bin range, bin centre (y_c) and measured cross section corrected to the electroweak Born level are shown. Other details as in Table 1.

Q^2 range (GeV ²)	Q_c^2 (GeV ²)	$d\sigma/dQ^2$ (pb/GeV ²)	N_{data}	$N_{\text{bg}}^{\text{MC}}$
185.0 – 300.0	250	$(1.06 \pm 0.00^{+0.01}_{-0.01}) \times 10^1$	67629	112.2
300.0 – 400.0	350	$(4.55 \pm 0.03^{+0.07}_{-0.03})$	19579	25.5
400.0 – 475.7	440	$(2.62 \pm 0.03^{+0.05}_{-0.04})$	8079	27.6
475.7 – 565.7	520	$(1.77 \pm 0.02^{+0.02}_{-0.05})$	5919	15.2
565.7 – 672.7	620	$(1.11 \pm 0.02^{+0.03}_{-0.03})$	4058	17.0
672.7 – 800.0	730	$(7.64 \pm 0.12^{+0.19}_{-0.25}) \times 10^{-1}$	3969	15.0
800.0 – 1050.0	900	$(4.41 \pm 0.06^{+0.09}_{-0.16}) \times 10^{-1}$	4994	19.7
1050.0 – 1460.0	1230	$(2.01 \pm 0.03^{+0.04}_{-0.05}) \times 10^{-1}$	3948	22.3
1460.0 – 2080.0	1730	$(8.25 \pm 0.17^{+0.27}_{-0.14}) \times 10^{-2}$	2485	10.9
2080.0 – 3120.0	2500	$(3.11 \pm 0.08^{+0.05}_{-0.06}) \times 10^{-2}$	1541	4.4
3120.0 – 5220.0	3900	$(8.54 \pm 0.30^{+0.15}_{-0.20}) \times 10^{-3}$	826	2.1
5220.0 – 12500.0	7000	$(1.43 \pm 0.08^{+0.02}_{-0.03}) \times 10^{-3}$	361	0.0
12500.0 – 51200.0	22400	$(1.93^{+0.35}_{-0.30} \text{ } ^{+0.11}_{-0.15}) \times 10^{-5}$	41	0.0

Table 12: The single-differential cross-section $d\sigma/dQ^2$ ($y < 0.9$, $y(1-x)^2 > 0.004$) for the reaction $e^+p \rightarrow e^+X$ ($\mathcal{L} = 56.7 \text{ pb}^{-1}$, $P_e = -0.36$). The bin range, bin centre (Q_c^2) and measured cross section corrected to the electroweak Born level are shown. Other details as in Table 1.

$Q^2 >$ (GeV ²)	x range	x_c	$d\sigma/dx$ (pb)	N_{data}	$N_{\text{bg}}^{\text{MC}}$
185	$(0.63 - 1.00) \times 10^{-2}$	0.794×10^{-2}	$(8.61 \pm 0.07^{+0.16}_{-0.16}) \times 10^4$	14173	69.1
	$(0.10 - 0.16) \times 10^{-1}$	0.126×10^{-1}	$(5.79 \pm 0.05^{+0.07}_{-0.17}) \times 10^4$	16410	50.8
	$(0.16 - 0.25) \times 10^{-1}$	0.200×10^{-1}	$(3.54 \pm 0.03^{+0.03}_{-0.03}) \times 10^4$	15901	33.4
	$(0.25 - 0.40) \times 10^{-1}$	0.316×10^{-1}	$(2.07 \pm 0.02^{+0.02}_{-0.01}) \times 10^4$	15715	12.7
	$(0.40 - 0.63) \times 10^{-1}$	0.501×10^{-1}	$(1.21 \pm 0.01^{+0.01}_{-0.01}) \times 10^4$	13656	2.3
	$(0.63 - 1.00) \times 10^{-1}$	0.794×10^{-1}	$(6.84 \pm 0.06^{+0.08}_{-0.03}) \times 10^3$	13087	2.1
	0.10 – 0.16	0.126	$(3.79 \pm 0.03^{+0.04}_{-0.01}) \times 10^3$	12219	0.7
	0.16 – 0.25	0.200	$(1.97 \pm 0.02^{+0.03}_{-0.06}) \times 10^3$	7505	0.0
3000	$(0.40 - 0.63) \times 10^{-1}$	0.501×10^{-1}	$(1.61 \pm 0.12^{+0.04}_{-0.05}) \times 10^2$	171	0.5
	$(0.63 - 1.00) \times 10^{-1}$	0.794×10^{-1}	$(1.50 \pm 0.09^{+0.05}_{-0.03}) \times 10^2$	277	1.7
	0.10 – 0.16	0.126	$(1.05 \pm 0.06^{+0.01}_{-0.05}) \times 10^2$	317	0.0
	0.16 – 0.25	0.200	$(5.81 \pm 0.36^{+0.11}_{-0.15}) \times 10^1$	259	0.0
	0.25 – 0.40	0.316	$(3.02 \pm 0.21^{+0.04}_{-0.09}) \times 10^1$	217	0.0
0.40 – 0.75	0.687	$(1.10 \pm 0.12^{+0.04}_{-0.02})$	89	0.0	

Table 13: The single-differential cross-section $d\sigma/dx$ ($y < 0.9$, $y(1-x)^2 > 0.004$) for $Q^2 > 185 \text{ GeV}^2$ and $Q^2 > 3000 \text{ GeV}^2$ for the reaction $e^+p \rightarrow e^+X$ ($\mathcal{L} = 56.7 \text{ pb}^{-1}$, $P_e = -0.36$). The Q^2 and bin range, bin centre (x_c) and measured cross section corrected to the electroweak Born level are shown. Other details as in Table 1.

$Q^2 >$ (GeV ²)	y range	y_c	$d\sigma/dy$ (pb)	N_{data}	$N_{\text{bg}}^{\text{MC}}$
185	0.00 – 0.05	0.025	$(1.60 \pm 0.01_{-0.01}^{+0.02}) \times 10^4$	30773	0.0
	0.05 – 0.10	0.075	$(7.98 \pm 0.06_{-0.04}^{+0.09}) \times 10^3$	20679	3.0
	0.10 – 0.15	0.125	$(5.53 \pm 0.05_{-0.04}^{+0.03}) \times 10^3$	14221	6.3
	0.15 – 0.20	0.175	$(4.34 \pm 0.04_{-0.14}^{+0.03}) \times 10^3$	10814	9.7
	0.20 – 0.25	0.225	$(3.55 \pm 0.04_{-0.20}^{+0.03}) \times 10^3$	8555	8.1
	0.25 – 0.30	0.275	$(2.89 \pm 0.04_{-0.05}^{+0.05}) \times 10^3$	6666	7.6
	0.30 – 0.35	0.325	$(2.47 \pm 0.03_{-0.04}^{+0.04}) \times 10^3$	5636	19.4
	0.35 – 0.40	0.375	$(2.24 \pm 0.03_{-0.03}^{+0.01}) \times 10^3$	5035	19.1
	0.40 – 0.45	0.425	$(1.95 \pm 0.03_{-0.02}^{+0.04}) \times 10^3$	4238	26.9
	0.45 – 0.50	0.475	$(1.68 \pm 0.03_{-0.02}^{+0.06}) \times 10^3$	3538	21.8
	0.50 – 0.55	0.525	$(1.52 \pm 0.03_{-0.02}^{+0.04}) \times 10^3$	3127	21.5
	0.55 – 0.60	0.575	$(1.38 \pm 0.03_{-0.04}^{+0.04}) \times 10^3$	2715	25.8
	0.60 – 0.65	0.625	$(1.26 \pm 0.03_{-0.04}^{+0.06}) \times 10^3$	2308	25.8
	0.65 – 0.70	0.675	$(1.18 \pm 0.03_{-0.05}^{+0.03}) \times 10^3$	1883	10.5
	0.70 – 0.75	0.725	$(1.11 \pm 0.03_{-0.05}^{+0.07}) \times 10^3$	1445	19.5
	0.75 – 0.90	0.825	$(9.24 \pm 0.22_{-0.46}^{+0.86}) \times 10^2$	1748	45.3
3000	0.05 – 0.10	0.075	$(2.99 \pm 0.37_{-0.04}^{+0.09}) \times 10^1$	65	0.0
	0.10 – 0.15	0.125	$(5.21 \pm 0.47_{-0.14}^{+0.05}) \times 10^1$	125	0.0
	0.15 – 0.20	0.175	$(5.33 \pm 0.46_{-0.07}^{+0.15}) \times 10^1$	132	0.0
	0.20 – 0.25	0.225	$(4.73 \pm 0.43_{-0.25}^{+0.09}) \times 10^1$	119	0.0
	0.25 – 0.30	0.275	$(4.19 \pm 0.40_{-0.15}^{+0.06}) \times 10^1$	108	0.0
	0.30 – 0.35	0.325	$(4.47 \pm 0.42_{-0.12}^{+0.07}) \times 10^1$	115	0.0
	0.35 – 0.40	0.375	$(3.54 \pm 0.37_{-0.21}^{+0.06}) \times 10^1$	91	0.0
	0.40 – 0.45	0.425	$(3.24 \pm 0.35_{-0.19}^{+0.04}) \times 10^1$	84	0.0
	0.45 – 0.50	0.475	$(3.61 \pm 0.37_{-0.24}^{+0.06}) \times 10^1$	93	0.0
	0.50 – 0.55	0.525	$(2.77 \pm 0.33_{-0.07}^{+0.06}) \times 10^1$	70	0.0
	0.55 – 0.60	0.575	$(2.64 \pm 0.33_{-0.06}^{+0.31}) \times 10^1$	66	0.0
	0.60 – 0.65	0.625	$(2.26 \pm 0.29_{-0.06}^{+0.16}) \times 10^1$	59	1.7
	0.65 – 0.70	0.675	$(1.72_{-0.27}^{+0.31} \pm 0.07_{-0.09}) \times 10^1$	42	0.0
	0.70 – 0.75	0.725	$(2.32 \pm 0.31_{-0.11}^{+0.05}) \times 10^1$	55	0.0
	0.75 – 0.80	0.775	$(2.05 \pm 0.30_{-0.14}^{+0.19}) \times 10^1$	48	0.0
	0.80 – 0.85	0.825	$(1.55_{-0.26}^{+0.31} \pm 0.27_{-0.07}) \times 10^1$	35	0.5
0.85 – 0.90	0.875	$(1.87_{-0.32}^{+0.37} \pm 0.19_{-0.12}) \times 10^1$	35	0.0	

Table 14: The single-differential cross-section $d\sigma/dy$ for $Q^2 > 185 \text{ GeV}^2$ and $Q^2 > 3000 \text{ GeV}^2$ ($y(1-x)^2 > 0.004$) for the reaction $e^+p \rightarrow e^+X$ ($\mathcal{L} = 56.7 \text{ pb}^{-1}$, $P_e = -0.36$). The Q^2 and bin range, bin centre (y_c) and measured cross section corrected to the electroweak Born level are shown. Other details as in Table 1.

Q^2 range (GeV ²)	Q_c^2 (GeV ²)	Ratio	Asymmetry A^+ $\times 10$
185.0 – 300.0	250	1.01 ± 0.01	0.18 ± 0.07
300.0 – 400.0	350	1.04 ± 0.01	0.57 ± 0.14
400.0 – 475.7	440	1.04 ± 0.02	0.59 ± 0.21
475.7 – 565.7	520	1.04 ± 0.02	0.54 ± 0.25
565.7 – 672.7	620	1.07 ± 0.02	0.95 ± 0.30
672.7 – 800.	730	1.05 ± 0.02	0.71 ± 0.30
800.0 – 1050.0	900	1.08 ± 0.02	1.09 ± 0.27
1050.0 – 1460.0	1230	1.05 ± 0.02	0.73 ± 0.30
1460.0 – 2080.0	1730	1.09 ± 0.03	1.27 ± 0.38
2080.0 – 3120.0	2500	1.05 ± 0.03	0.77 ± 0.48
3120.0 – 5220.0	3900	1.21 ± 0.05	2.82 ± 0.63
5220.0 – 12500.0	7000	1.21 ± 0.08	2.74 ± 0.95
12500.0 – 51200.0	22400	1.05 ± 0.21	0.76 ± 2.96

Table 15: *The polarisation asymmetry measured using positively and negatively polarised e^+p beams ($\mathcal{L} = 78.8 \text{ pb}^{-1}$, $P_e = +0.32$ and $\mathcal{L} = 56.7 \text{ pb}^{-1}$, $P_e = -0.36$, respectively). The bin range, bin centre (Q_c^2), the cross section ratio of the samples with $P_e = +0.32$ and $P_e = -0.36$ and the measured asymmetry A^+ are shown. Only the statistical uncertainties on the measurement are shown as systematic uncertainties are assumed to cancel.*

ZEUS

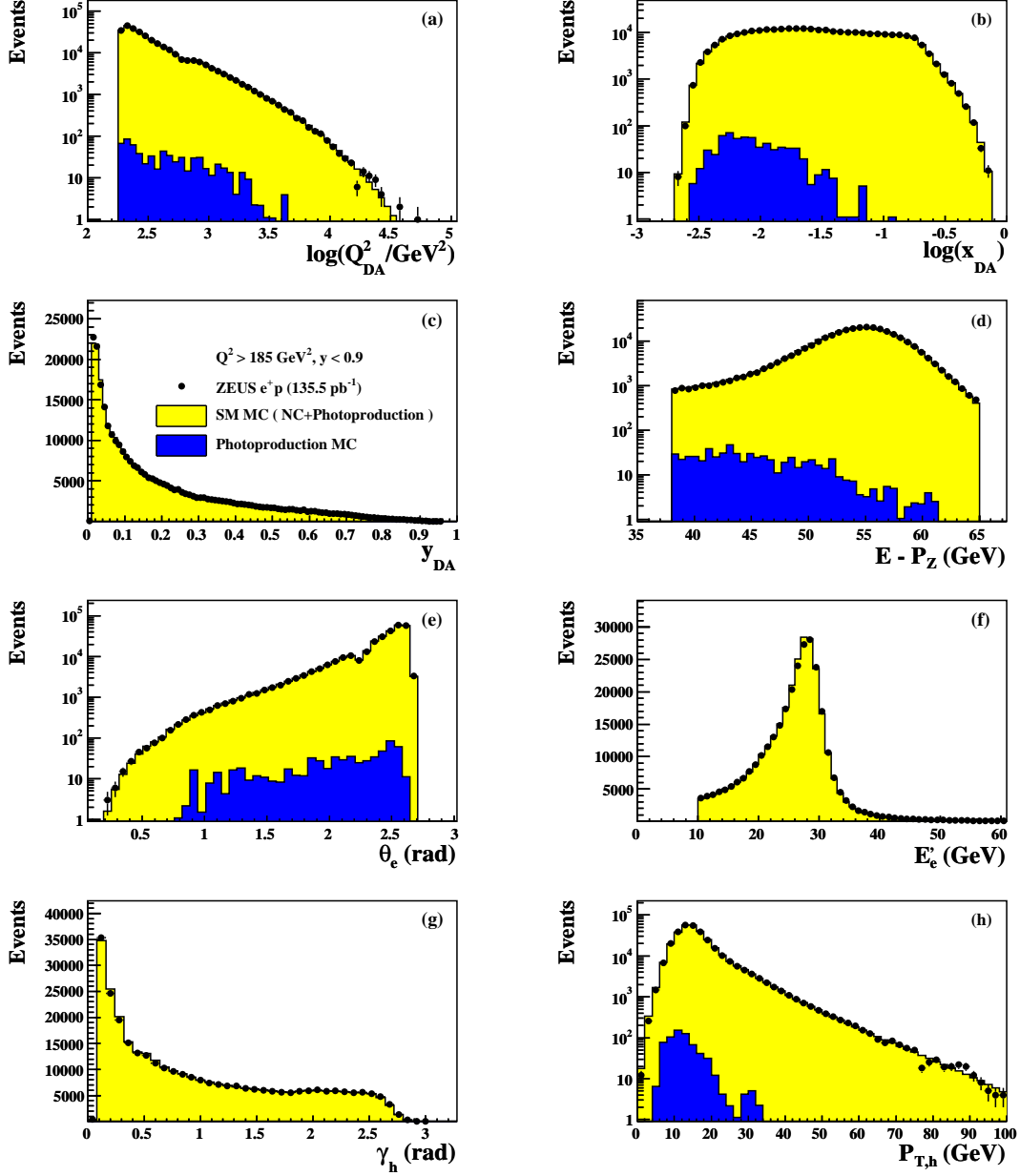


Figure 1: Comparison of the e^+p NC data sample with the predictions from the MC simulation. The MC distributions are normalised to the data luminosity. The distributions of (a) Q_{DA}^2 , (b) x_{DA} , (c) y_{DA} , (d) $E - P_Z$, (e) θ_e , (f) E'_e , (g) γ_h and (h) $P_{T,h}$ are shown.

ZEUS

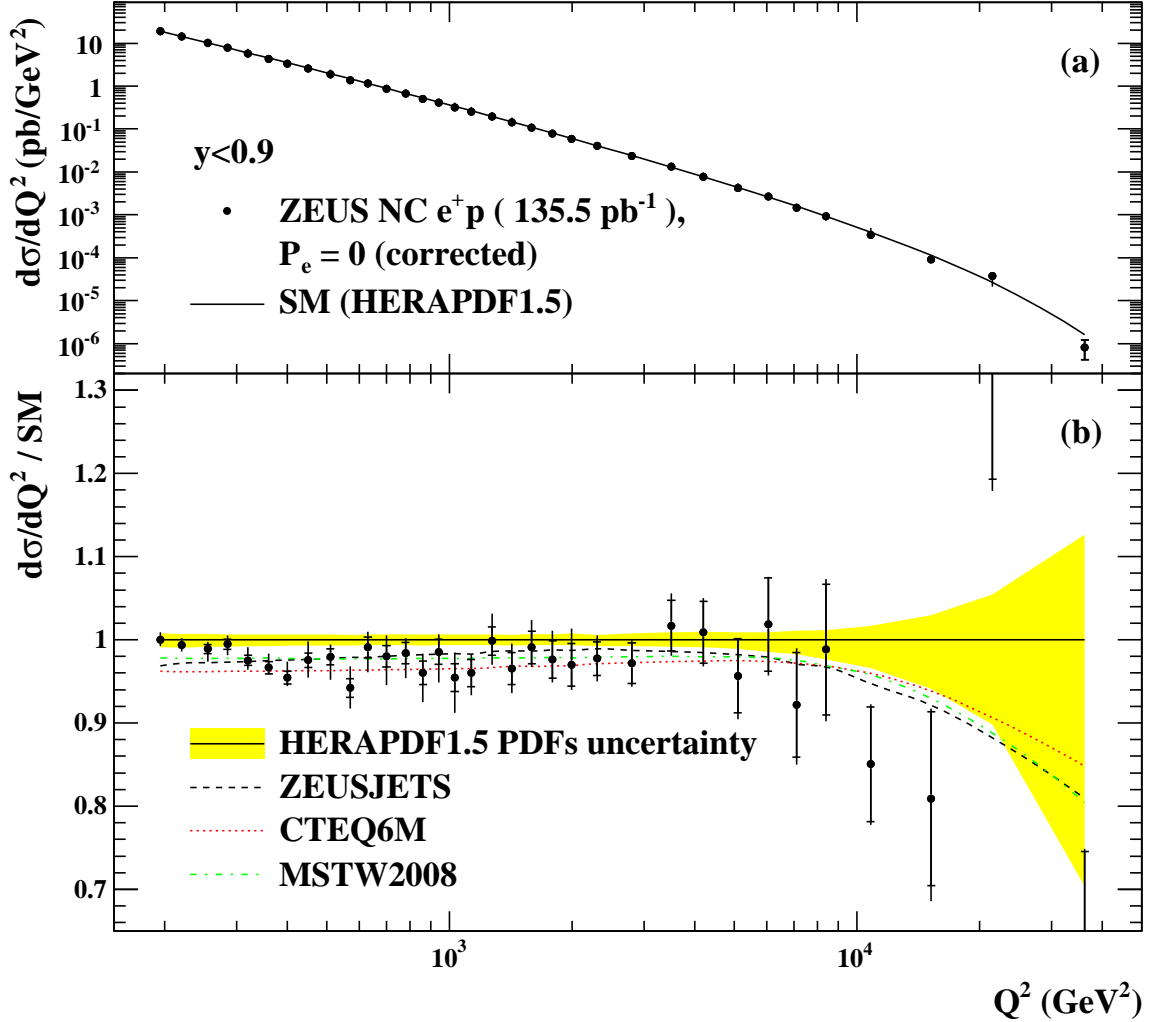


Figure 2: (a) The e^+p NC DIS cross-section $d\sigma/dQ^2$ for $y < 0.9$ and $y(1-x)^2 > 0.004$ corrected to $P_e = 0$ and (b) the ratio to the SM prediction. The closed circles represent data points in which the inner error bars show the statistical uncertainty while the outer bars show the statistical and systematic uncertainties added in quadrature. The curves show the predictions of the SM evaluated using the HERAPDF1.5 PDFs and the shaded band shows the uncertainties from the HERAPDF1.5 PDFs. In the ratio plot in addition the ratios between other PDFs (ZEUSJETS (dashed), CTEQ6M (dotted) and MSTW2008 (dash-dotted)) and HERAPDF1.5 are shown as curves. The uncertainties of CTEQ6M and MSTW2008 are of the same order as of HERAPDF1.5, the uncertainties of ZEUSJETS are about a factor 2 higher.

ZEUS

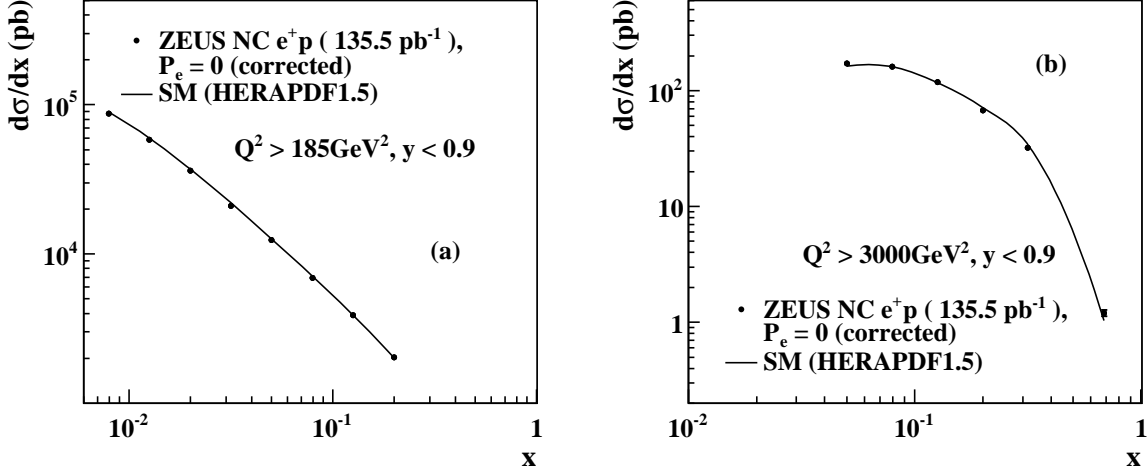


Figure 3: The e^+p NC DIS cross-section $d\sigma/dx$ for (a) $Q^2 > 185 \text{ GeV}^2$ and (b) $Q^2 > 3000 \text{ GeV}^2$ for $y < 0.9$ and $y(1-x)^2 > 0.004$. The closed circles represent data points in which the inner error bars show the statistical uncertainty while the outer bars show the statistical and systematic uncertainties added in quadrature. The curves show the predictions of the SM evaluated using the HERAPDF1.5 PDFs.

ZEUS

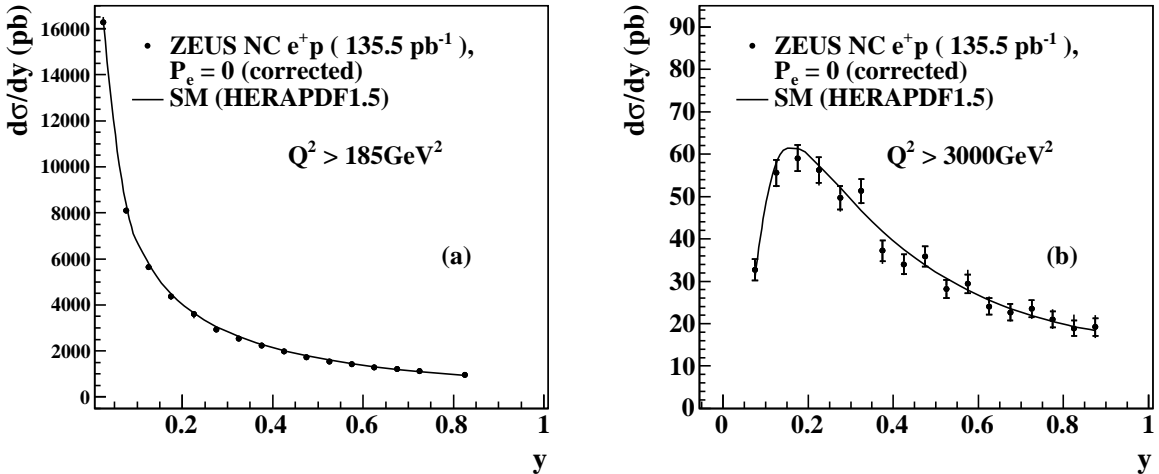


Figure 4: The e^+p NC DIS cross-section $d\sigma/dy$ for (a) $Q^2 > 185 \text{ GeV}^2$ and (b) $Q^2 > 3000 \text{ GeV}^2$ for $y(1-x)^2 > 0.004$. Other details as in Figure 3.

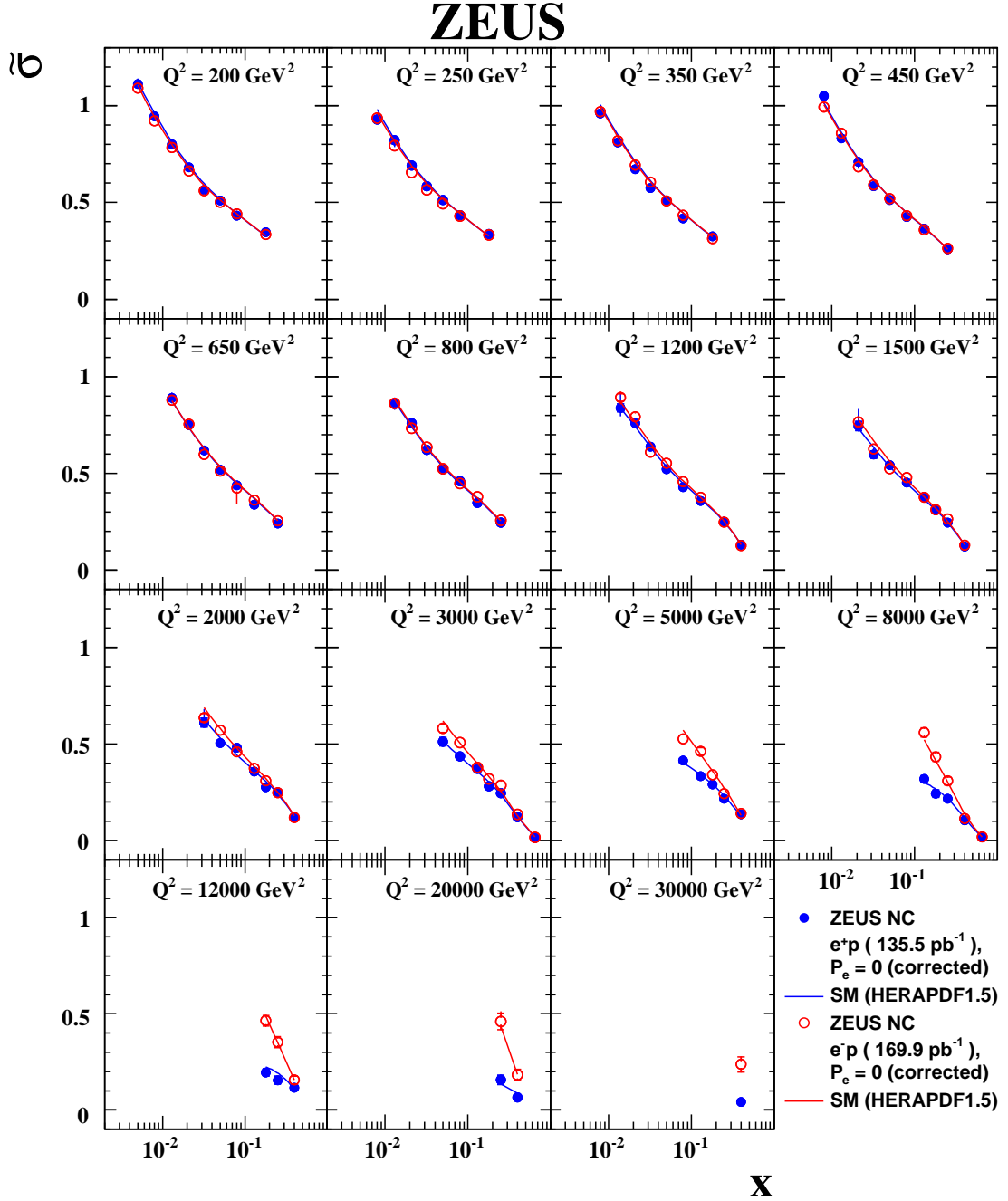


Figure 5: The $e^\pm p$ unpolarised NC DIS reduced cross-section $\tilde{\sigma}$ plotted as a function of x at fixed Q^2 . The closed (open) circles represent data points for e^+p (e^-p) collisions in which the inner error bars show the statistical uncertainty while the outer bars show the statistical and systematic uncertainties added in quadrature, although errors are too small to be seen in most cases. The curves show the predictions of the SM evaluated using the HERAPDF1.5 PDFs.

ZEUS

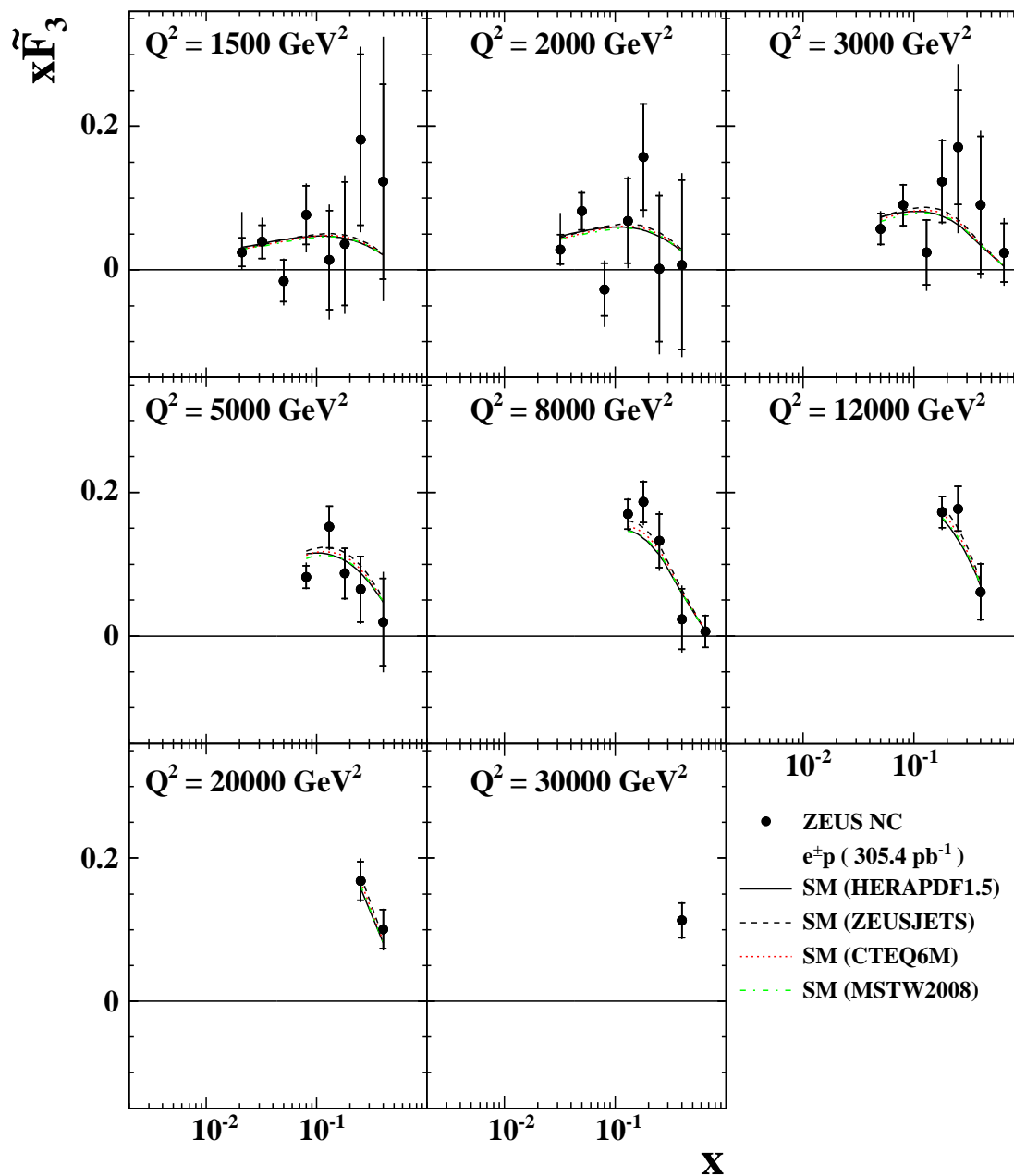


Figure 6: The structure-function $x\tilde{F}_3$ plotted as a function of x at fixed Q^2 . The closed circles represent the ZEUS data. The inner error bars show the statistical uncertainty while the outer ones show the statistical and systematic uncertainties added in quadrature. The curves show the predictions of the SM evaluated using HERAPDF1.5 (solid), ZEUSJETS (dashed), CTEQ6M (dotted) and MSTW2008 (dash-dotted) PDFs.

ZEUS

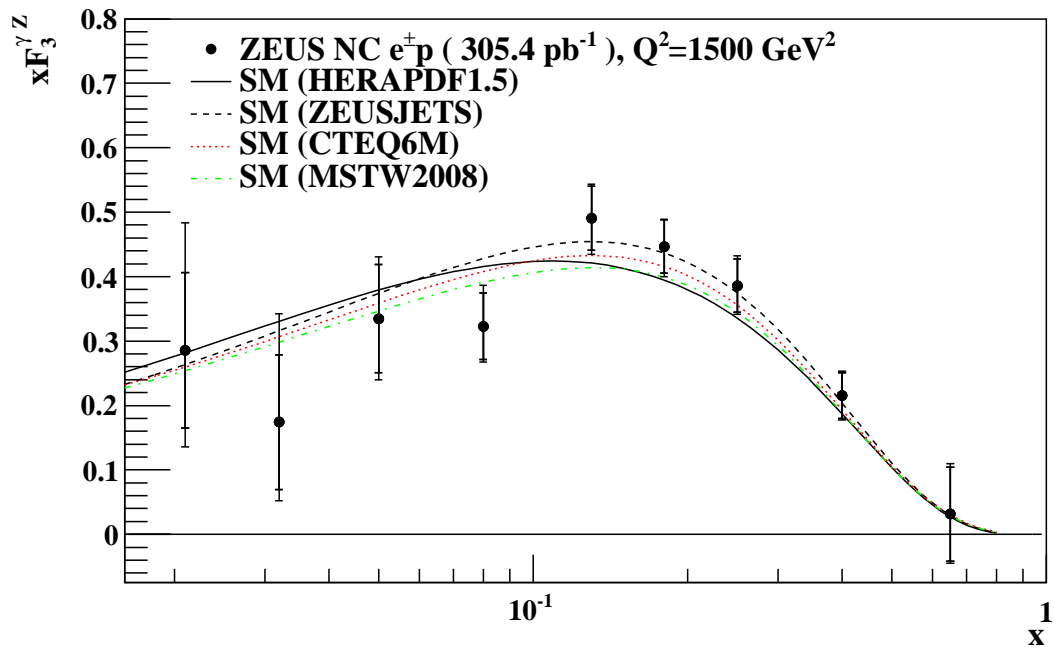


Figure 7: The structure function $x F_3^{\gamma Z}$ extrapolated to a single Q^2 value of 1500 GeV² and plotted as a function of x . Other details as in Figure 6.

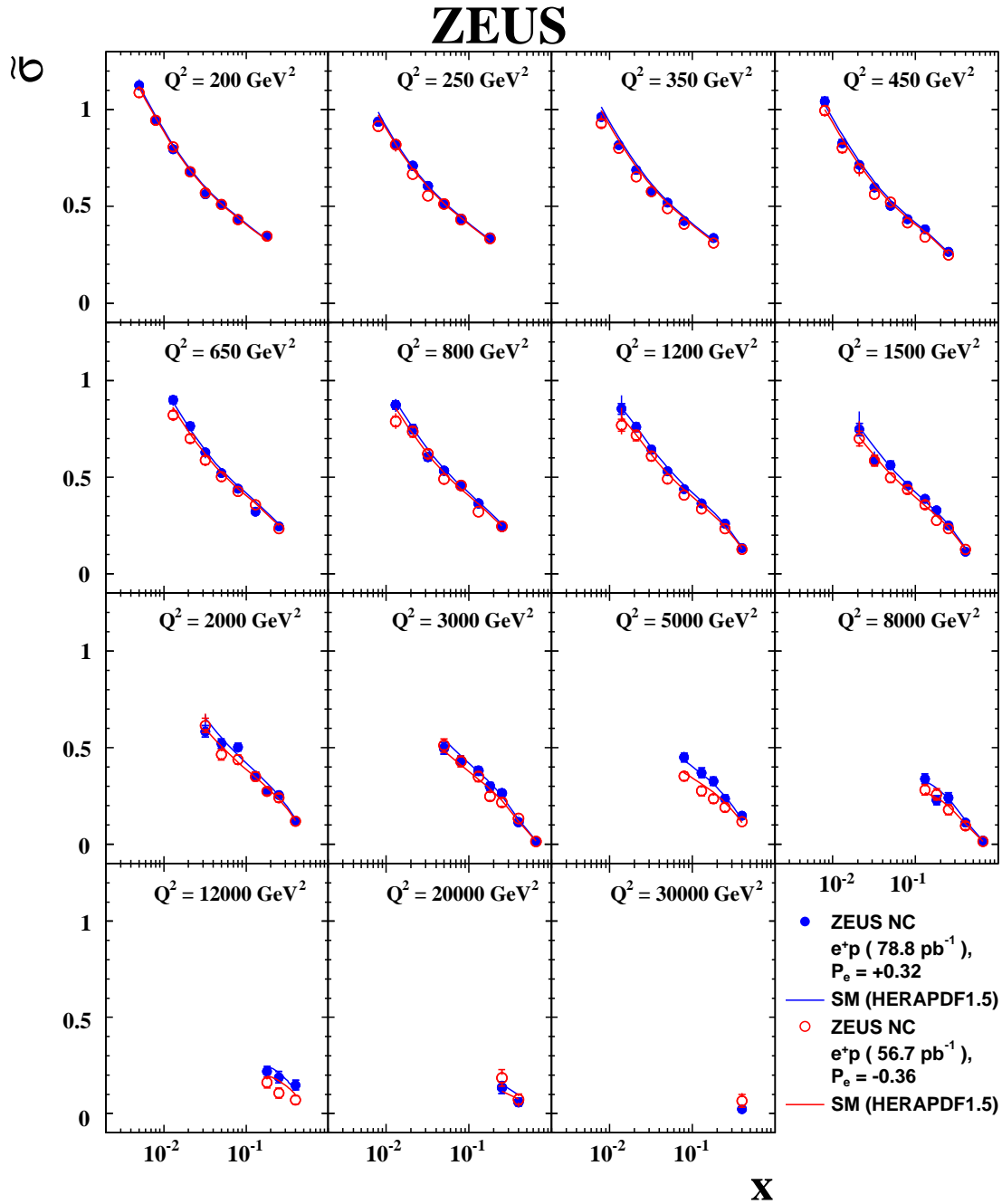


Figure 8: The e^+p NC DIS reduced cross-section $\tilde{\sigma}$ for positively and negatively polarised beams plotted as a function of x at fixed Q^2 . The closed (open) circles represent the ZEUS data for negative (positive) polarisation. Other details as in Figure 5.

ZEUS

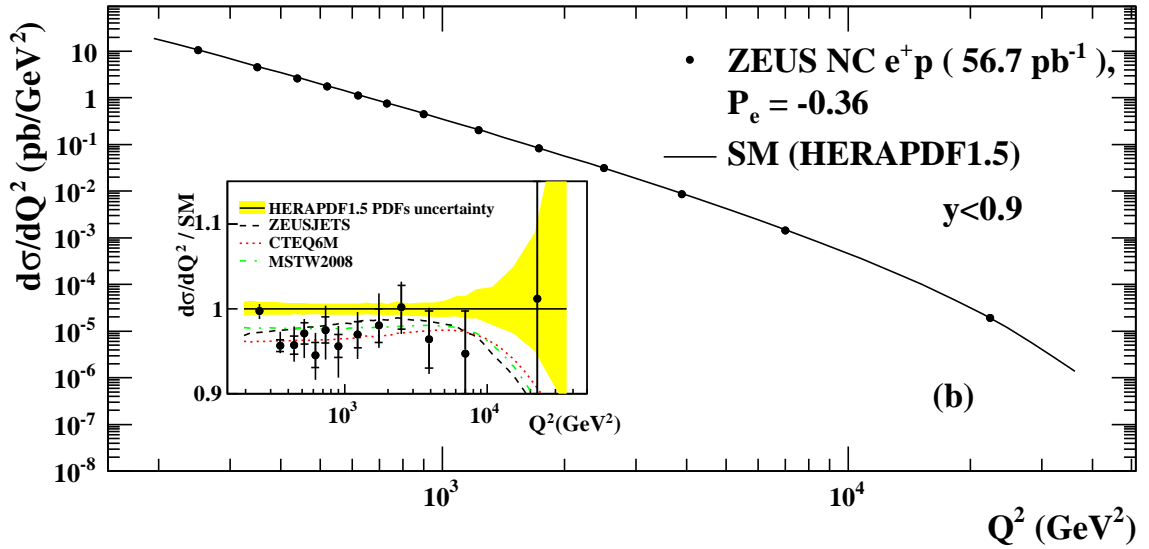
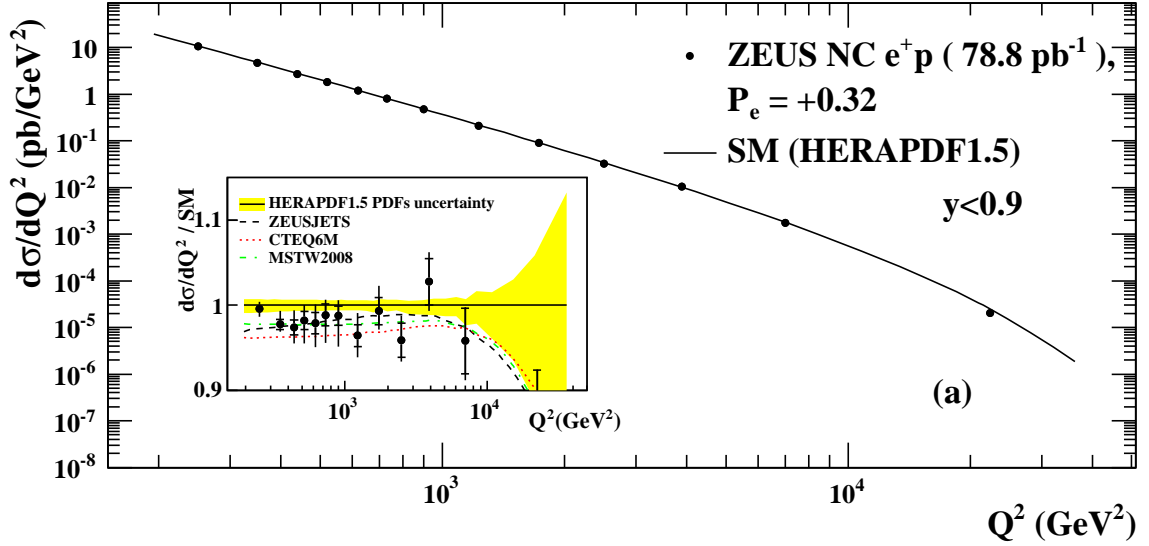


Figure 9: The e^+p NC DIS cross-section $d\sigma/dQ^2$ for $y < 0.9$ and $y(1-x)^2 > 0.004$ for (a) positive and (b) negative polarisation. Other details as in Figure 2.

ZEUS

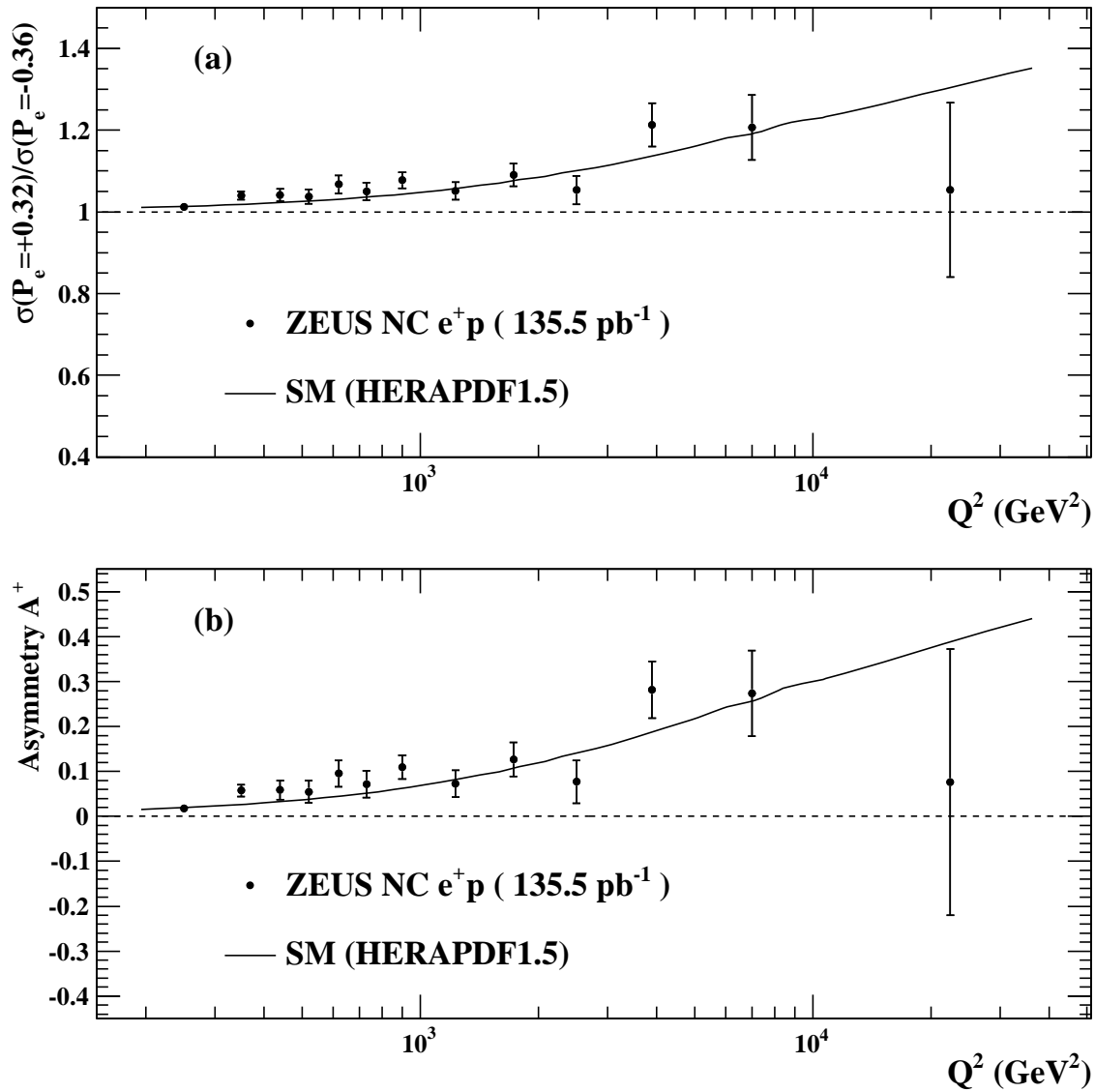


Figure 10: The (a) ratio of $d\sigma/dQ^2$ using positive and negative polarisation and (b) the polarisation asymmetry A^+ as functions of Q^2 . The closed circles represent ZEUS data. Only statistical uncertainties are considered as the systematic uncertainties are assumed to cancel. The curves show the predictions of the SM evaluated using the HERAPDF1.5 PDFs.